METHOD OF SYNCHRONIZATION USING IEEE 802.11a OFDM TRAINING STRUCTURE FOR INDOOR WIRELESS APPLICATIONS

by

Cheuk Kwan Lui

B.S.E.E., California State University, Fresno, 1991

PROJECT SUBMITTED IN PARTIAL FULFILLMENT OF
THE REQUIREMENTS FOR THE DEGREE OF
MASTER OF ENGINEERING

In the School
of
Engineering Science

SIMON FRASER UNIVERSITY

Fall 2004

APPROVAL

Name: **Cheuk Kwan Lui**

Degree: **Master of Engineering**

Title of Project: **Method of Synchronization using IEEE 802.11a OFDM Training Structure for Indoor Wireless Applications**

Examining Committee:

Chair: _____

Dr. Dong In Kim
Associate Professor

_____

Dr. Paul Ho
Senior Supervisor
Professor

_____

Dr. James K. Cavers
Supervisor
Professor

Date Approved: Nov. 22. 2004

SIMON FRASER UNIVERSITY

PARTIAL COPYRIGHT LICENCE

ABSTRACT

IEEE standard 802.11a supports the new high rate physical layer OFDM (Orthogonal Frequency Division Multiplexing) wireless LAN system for operation in the 5GHz unlicensed national information infrastructure (U-NII) band. The OFDM physical layer specifies PPDU (PLCP protocol data unit) frame format that consists of PLCP (Physical Layer Convergence Procedure) preamble, the PLCP header, PSDU, Tail bits and Pad bits. The PLCP preamble is the major component for synchronization, and it consists of 10 "Short" OFDM symbols and 2 "Long" OFDM symbols. This project focuses on researching robust synchronization methods for 802.11a OFDM systems using the PLCP "Short" and "Long" training symbols. Monte Carol simulations are applied to evaluate the performance of the proposed methods of synchronization in AWGN (Additive White Gaussian Noise) channel and indoor residential channel using JTC (Joint Technical Committee) wireless channel model.

DEDICATION

To my parents, my lovely wife Carmen, and my family. Thanks for all the loves and supports throughout the years of supporting my study.

ACKNOWLEDGEMENTS

I give special thanks to Dr. Paul Ho for his valuable time and guidance in assisting me to complete my project. His challenging questions invoked my thinking and encouraged me to face difficult tasks. Also, I say thank you to Dr. James K. Cavers for his teaching and his time in sharing and providing comments on my project.

Thanks to IEEE for permission to use their descriptions and figures with the following notice: Fig. 107 PPDU Frame format, Fig. 110 OFDM Training Structure reprinted with permission from IEEE Std 802.11a-1999, "Supplement to IEEE standard for information technology telecommunications and information exchange between systems - local and metropolitan area networks - specific requirements. Part 11: wireless LAN Medium Access Control (MAC) and Physical Layer (PHY) specifications: high-speed physical layer in the 5 GHz band" Copyright 1999 by IEEE. The IEEE disclaims any responsibility or liability resulting from the placement and use in the described manner.

Many thanks to the persons who have encouraged and supported my study, including my family, my wife Carmen, and my friends, teachers and colleagues past and present.

TABLE OF CONTENTS

LIST OF FIGURES

LIST OF TABLES

LIST OF ABBREVIATIONS AND ACRONYMS

ADSL	Asymmetric Digital Subscriber Line
AWGN	Additive White Gaussian Noise
BER	Bit Error Rate
BPSK	Binary Phase –Shift Keying
DAB	Digital Audio Broadcasting
DMT	Discrete Multi-tone
DVB	Digital Video Broadcasting
FER	Frame Error Rate
GI	Guard Interval
HDSL	High-speed Digital Subscriber Line
HDTV	High Definition Television
ICI	Inter Channel Interference
IDFT	Inverse Discrete Fourier Transformer
IFFT	Inverse Fast Fourier Transformer
ISI	Inter Symbol Interference
JTC	Joint Technical Committee
LAN	Local Area Network
LOS	Line of Sight
MCM	Multi-carrier Modulation
MLE	Maximum Likelihood Estimation
MPSK	M-ary Phase –Shift Keying

MSE	Mean Square Error
NLOS	Near Line of Sight
OFDM	Orthogonal Frequency Division Multiplexing
PAPR	Peak-to-Average Power Ratio
PLCP	Physical Layer Convergence Procedure
PMD	Physical Medium Dependent
PN	Pseudonoise
PPDU	PLCP Protocol Data Unit
PSDU	Physical Sublayer Service Data Units
QPSK	Quadrature Phase –Shift Keying
TOA	Time of Arrival
U-NII	Unlicensed National Information Infrastructure
WLAN	Wireless Local Area Network

1. INTRODUCTION

Reliable and effective communication depends on successful transmission and reception of information data through an imperfect channel. In wireless communication systems, transmitters and receivers are not physically connected and that introduce lot more difficulties in establishing effective communication links. A wireless channel introduces unwanted noises on the data during transmission, and the signal levels fluctuate with noises depending on the strengths of the signal and the surrounding interferences. In addition, wireless Local Area Network (WLAN) systems involve high volumes of digital data that require more reliable synchronization clock systems and robust frame synchronizers in order to establish effective communication links by reducing the inter symbol interference (ISI) and inter carrier interference (ICI) of the data. The higher the speed of the data, the more accurate the clocks and carrier frequencies are required for synchronization.

1.1 Orthogonal Frequency Division Multiplexing

Orthogonal Frequency Division Multiplexing (OFDM) is a bandwidth efficient signalling scheme, which has been in existence for decades, and was first proposed by Chang for digital communication [1]. Recently, OFDM techniques are highly deployed in high-speed digital data transmission world, such as in Asymmetric Digital Subscriber Line (ADSL), High-speed Digital Subscriber Line (HDSL), Digital Audio Broadcasting (DAB), Digital Video Broadcasting (DVB), High Definition Television (HDTV) terrestrial broadcasting, Wireless LAN, and Cable systems.

OFDM is a form of Multi-carrier Modulation (MCM), that is an approach to divide a single serial transmission channel into a number of orthogonal parallel subchannels or subcarriers to optimize the efficiency of data transmission. Orthogonal Frequency Division Multiplexing (OFDM) and Discrete Multi-tone (DMT) are different forms of MCM.

In a single carrier modulation system, serial data is modulated in a high frequency carrier and transmitted through a single channel. The data rate is limited by the serial operation during transmission. In order to overcome the limitation in the single carrier modulation, MCM is to divide a single serial transmission channel into a number of orthogonal parallel subchannels or subcarriers for data transmission.

OFDM gives an optimum spectrum efficiency using mutually overlapped carriers [5]. OFDM signalling is proven to be an effective way to combat the negative effects of fading and multipath by dividing the frequency selective fading channel into a number of flat fading subchannels corresponding to the OFDM subcarrier frequencies [4].

In OFDM systems, ISI and ICI can be entirely eliminated by the simple expedient of inserting between symbols a small time interval known as a guard interval (GI). The length of the guard interval is made equal to or greater than the time spread of the channel. If the symbol waveform is extended periodically with the guard interval, the orthogonality is maintained over the symbol period, thus eliminating ICI. ISI is also eliminated by the non-overlapping symbols due to the guard interval [5].

When OFDM systems are compared to single carrier systems, channel equalization is less complex, and sensitivity to channel estimation, and frame synchronization error is reduced [4].

However, the major weakness of OFDM systems is highly sensitive to frequency offset in the channel than in single carrier systems. Therefore, a reliable synchronization method is significant to OFDM systems.

1.2 OFDM Synchronization

In designing OFDM systems, time and frequency synchronization are crucial in order to achieve a high performance of data transmission. One issue is the unknown arrival time of the OFDM symbol. Time shift of the received OFDM data frame causes frame synchronization errors. A symbol timing offset causes a linear phase rotation of the receiver FFT outputs and introduces ISI [4][8]. However, insertion of Guard Interval eliminates the overlapping between successive symbols to improve ISI.

The second issue is the frequency offset in the channel caused by tuning oscillator inaccuracies and Doppler shifts. The frequency offset causes the reduction of signal amplitudes in the output of the filters matched to each of the carriers, and introduces ICI from the other carriers that are now no longer orthogonal. The tolerable frequency offset is a very small fraction of the channel bandwidth due to the OFDM carriers are inherently closely spaced in frequency compared to the channel bandwidth. Maintaining sufficient open loop frequency accuracy is difficult in mobile radio links that introduce significant Doppler shift [5].

OFDM synchronization refers to maintain the orthogonality, and to combat against ISI and ICI between the multiplexed signals by tackling time offset error and carrier frequency offset (CFO) error. A robust synchronization scheme in OFDM systems provides an optimum performance by correctly estimating the arrival time of the signal,

the start position of data frames, and the time offset error to align the frame reception of symbols with successfully guard interval removal; and tracking the carrier frequency offset precisely. Redundancy in the OFDM frame structure and special training symbols provide means for synchronization.

Frequency synchronization is usually performed in two stages – frequency acquisition and frequency tracking – to reduce overall complexity. Frequency acquisition generates a coarse frequency estimate in a quick manner, and frequency tracking handles locking and tracking tasks in an accurate manner [6].

In the past years, several papers have been published to tackle the subject of synchronization for OFDM systems. Paul H. Moose [5] proposed Maximum Likelihood Estimation (MLE) Algorithm for carrier frequency offset estimation; Van de Beek [7] provided another solution using Joint Maximum Likelihood Algorithm for symbol time and carrier frequency. Timothy M. Schmidl [9] mentioned in his paper the importance of finding the start of the frame, and he introduced a timing metric to determine the start of the frame in addition to his algorithm to estimate the symbol timing and carrier frequency offset. Therefore, the estimation of the start of the frame, symbol timing and carrier frequency offset are the major elements in designing a robust OFDM system.

1.3 Wireless OFDM System

Wireless systems face more challenging problems in a multipath channel. In a multipath channel, the direct path signal and many reflected signals arrive at the receiver at different time delays with random phase distortions. The multipath signals cause ISI,

especially in high data rate transmission, when a symbol is distorted by the previously transmitted symbol.

In a wireless OFDM system, the technique used to combat against the multipath fading channel is converting a high–speed data channel into several slow parallel narrowband subchannels; or in other word, the technique lengthens the symbol period. As a result, the delay spread of multipath signal is suppressed to within a symbol period.

2. IEEE 802.11A STANDARD [2][1]

OFDM has been exploited extensively in digital communication world. IEEE Wireless LAN Working Group proposed and released a new standard 802.11a for wireless LAN system in 1999. The following has been summarized from the IEEE 802.11a Standard.

The 802.11a standard supports the new high rate physical layer OFDM wireless LAN system for operation in the 5GHz unlicensed national information infrastructure (U-NII) band. The OFDM system provides a wireless LAN with data payload communication capabilities of 6, 9, 12, 18, 24, 36, 48, and 54 Mbit/s. The support of transmitting and receiving at data rates of 6, 12, and 24 Mbit/s is mandatory. The system uses 52 subcarriers that are modulated using binary or quadrature phase shift keying (BPSK/QPSK), 16-quadrature amplitude modulation (QAM), or 64-QAM. Forward error correction coding (convolutional coding) is used with a coding rate of 1/2, 2/3, or 3/4.

The PPDU (PLCP protocol data unit) frame format defines the data packet structure in the 802.11a standard. A special training structure defined in the PLCP (Physical Layer Convergence Procedure) preamble field of the PPDU frame format is used for synchronization. The PLCP preamble consists of 10 "Short" symbols and 2 "Long" symbols. The 10 "Short" symbols are used for signal detection, AGC, diversity selection, coarse frequency offset estimation and timing

---

[1] From IEEE Std. 802.11a-1999. Copyright 1999 by IEEE. All rights reserved. This description is reprinted and summarized by permission of IEEE, "Supplement to IEEE standards for information technology telecommunications and information exchange between systems - local and metropolitan area networks - specific requirements. Part 11: wireless LAN Medium Access control (MAC) and Physical layer (PHY) specifications: high-speed physical layer in the 5 GHz band." The IEEE disclaims any responsibility or liability resulting from the placement and use in the described manner.

synchronization. The 2 "Long" symbols are used for channel and fine frequency offset estimation.

2.1 IEEE 802.11a Physical Layer [2][2]

2.1.1 PPDU Frame Format

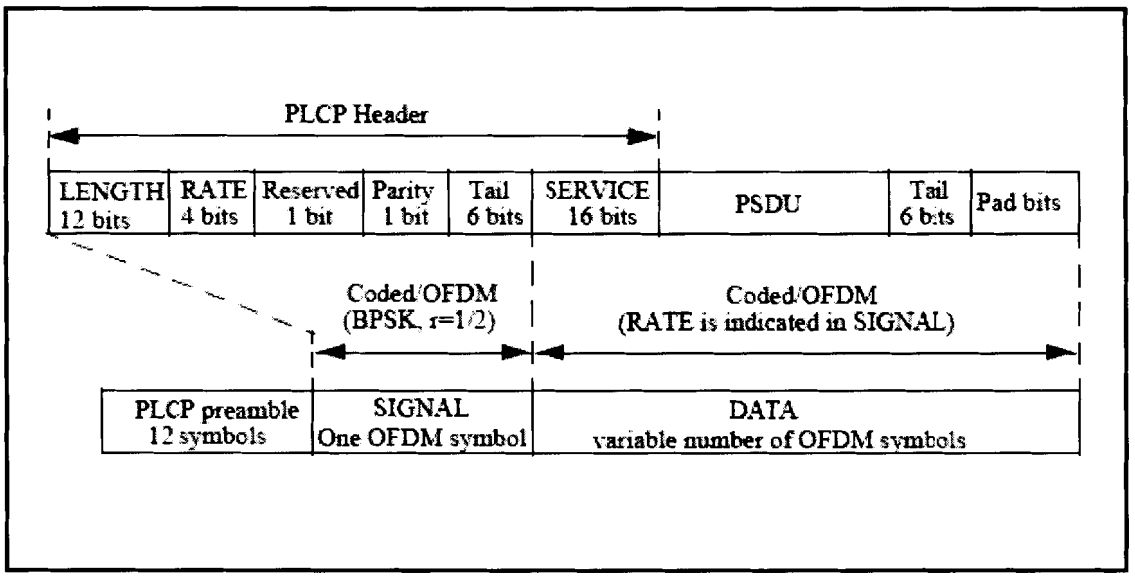

Figure 1 – 802.11a PPDU Frame Format, ©1999 IEEE Std. 802.11a-1999, by permission

The OFDM physical layer described in IEEE 802.11a 5GHz OFDM WLAN system consists of two protocol functions - a physical convergence function and a PMD (physical medium dependent) system. The PLCP supports a physical convergence function. PLCP defines a method of mapping the IEEE 802.11a physical sublayer service data units (PSDU) into a framing format suitable for sending and receiving user data and management information between two or more stations using the associated PMD system. A PMD system function defines

[2] From IEEE Std. 802.11a-1999. Copyright 1999 by IEEE. All rights reserved. This description and figure (Fig. 107 in the original) are reprinted and summarized by permission of IEEE, "Supplement to IEEE standards for information technology telecommunications and information exchange between systems - local and metropolitan area networks - specific requirements. Part 11: wireless LAN Medium Access control (MAC) and Physical layer (PHY) specifications: high-speed physical layer in the 5 GHz band."The IEEE disclaims any responsibility or liability resulting from the placement and use in the described manner.

the characteristics and method of transmitting and receiving data through a wireless medium between two or more stations, each using the OFDM system.

PPDU frame format, described in Figure 1, includes the OFDM PLCP preamble, OFDM PLCP header, PSDU, tail bits, and pad bits. The PLCP header contains the following fields: LENGTH, RATE, a reserved bit, an even parity bit, and the SERVICE field. The SIGNAL field is composed of the information bits containing the LENGTH, RATE, reserved bit, and parity bit (with 6 "zero" tail bits appended); and the SIGNAL is transmitted with BPSK modulation and a coding rate of R = 1/2. The DATA field contains the SERVICE field of the PLCP header and the PSDU (with 6 "zero" tail bits and pad bits appended); and the DATA may constitute multiple OFDM symbols that are transmitted at the data rate described in the RATE field. The tail bits in the SIGNAL symbol enable decoding of the RATE and LENGTH fields immediately after the reception of the tail bits. The RATE and LENGTH are required for decoding the DATA part of the packet.

2.1.2 OFDM Training Structure[3]

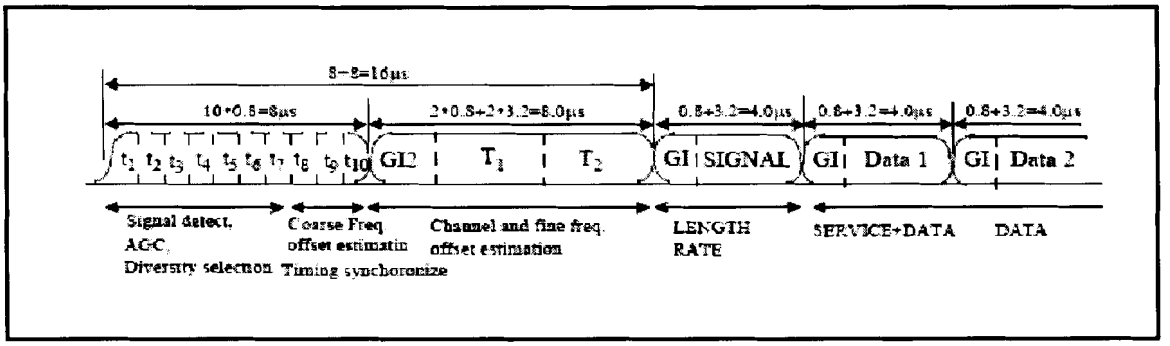

Figure 2 – 802.11a OFDM Training Structure, ©1999 IEEE Std. 802.11a-1999, by permission

---

[3] From IEEE Std. 802.11a-1999. Copyright 1999 by IEEE. All rights reserved. This description and figure (Fig. 110 in the original) are reprinted and summarized by permission of IEEE, "Supplement to IEEE standards for information technology telecommunications and information exchange between systems - local and metropolitan area networks - specific requirements. Part 11: wireless LAN Medium Access control (MAC) and Physical layer (PHY) specifications: high-speed physical layer in the 5 GHz band."The IEEE disclaims any responsibility or liability resulting from the placement and use in the described manner.

The PLCP preamble field, shown in Figure 2, consists of totally 12 symbols, including 10 "short training sequence" and 2 "Long training sequence", are designed for synchronization between the transmitter and the receiver. Each "Short training sequence" represents an OFDM "Short" symbol of 0.8μs long, and each "Long training sequence" represents an OFDM "Long" Symbol of 3.2μs long. The ten repetitions of the "Short training sequence" are used for signal detection, AGC convergence, diversity selection, timing acquisition, and coarse frequency acquisition. The two repetitions of a "Long training sequence", preceded by a guard interval (GI), are used for channel estimation and fine frequency acquisition in the receiver.

The guard interval is used for shifting the time to create the "circular prefix" used in OFDM to avoid ISI from the previous frame. The "Short training sequence" has no guard interval. The "Long training sequence" has the longest guard interval of 3.2μs. The guard intervals in the "Signal" and "Data" fields are only 1.6μs.

The Summary above provides a brief introduction of the IEEE 802.11a OFDM system, and describes the details of the frame structure and the OFDM training structure for synchronization. The following study about the system synchronization utilizes the frame structure and the training structure described in the IEEE 802.11a OFDM standard.

3. OFDM SYSTEM MODEL

3.1 Model Structure [10]

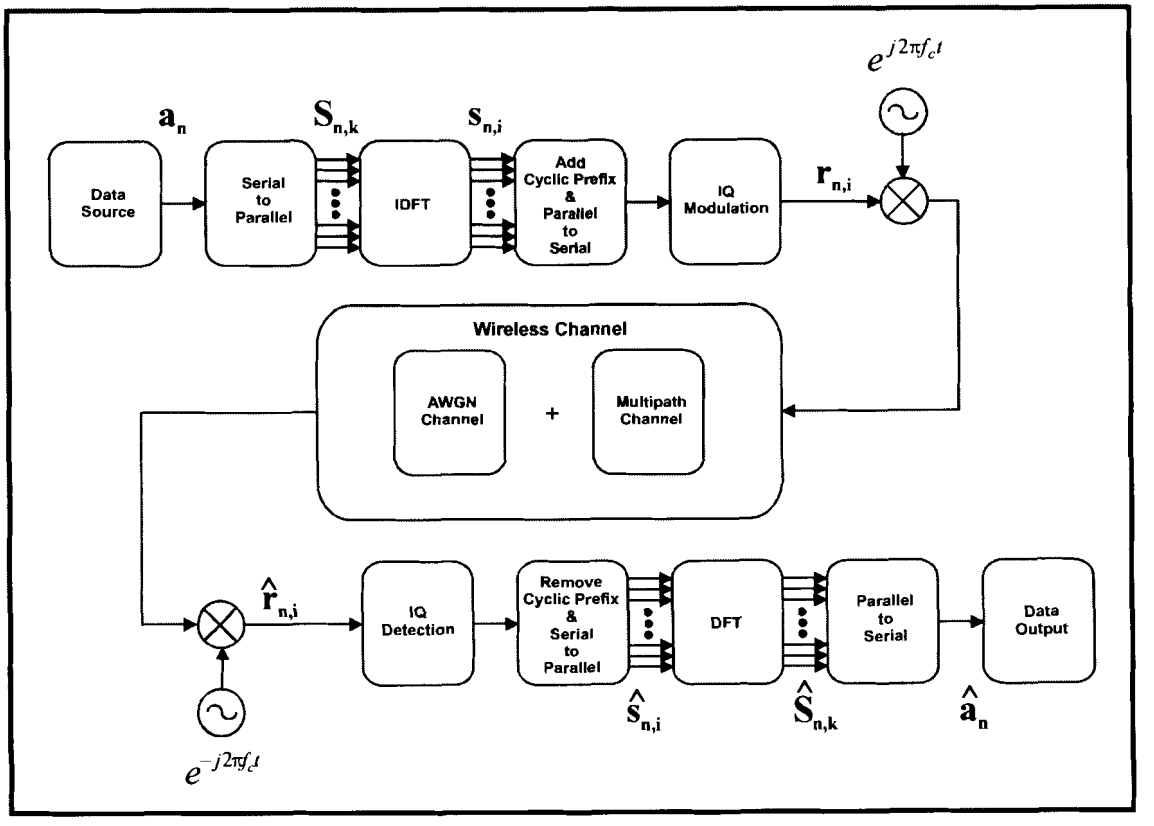

Figure 3 – OFDM System Model

An OFDM system modelled as in Figure 3 has N subcarriers spaced by the frequency distance Δf. Thus, the bandwidth of the system is $B = N \cdot \Delta f$. All subcarriers are mutually orthogonal within a time interval of length $T_s = 1/\Delta f$. Since the bandwidth equals to $N \cdot \Delta f$, the sampling time of the system must be $\Delta t = 1/(N \cdot \Delta f)$. The samples of the OFDM signal $s_{n,i}$ at discrete time $i = 0,1,...,N-1$ are represented by

$$s_{n,i} = \frac{1}{\sqrt{N}} \sum_{k=0}^{N-1} S_{n,k} e^{j\frac{2\pi ki}{N}} \quad \textbf{(1)}$$

where $S_{n,k}$ is the OFDM symbol data at the k-th subcarrier of the n-th frame, i is the i-th discrete time slot, k is the k-th subcarrier, and N is the total number of subcarriers.

Generation of the OFDM samples takes place at the transmitter through several conversions. Firstly, a serial data bit stream, in forms of BPSK, QPSK, 16-QAM, or 64-QAM subsymbols, is converted to parallel data. The subsymbols are in form of complex baseband data consists of in-phase and quadrature components $A_{n,k}$ and $B_{n,k}$ respectively.

$$S_{n,k} = A_{n,k} + jB_{n,k} \quad \textbf{(2)}$$

Then, taking the Inverse Discrete Fourier Transform (IDFT) of the parallel baseband data generates the OFDM signal samples. Inverse Fast Fourier Transform (IFFT) is a common conversion method for IDFT. Finally, the Cyclic Prefix, also known as the Guard Interval, is added to the parallel OFDM samples before converting them back to serial data for transmission. Insertion of Cyclic Prefix is achieved by attaching a number of samples, that equals to the length of the Cyclic Prefix, from the end portion of the parallel IDFT converted data to the front of itself.

3.2 Time Offset

Detection of the arrival of the OFDM data frame depends on searching the 10 repetitive training "Short" symbols for synchronization. Estimation of the frame start position determines the alignment of the FFT-window to detect the OFDM symbol in the

receiver. A false estimate leads to ISI which may disturb the orthogonality of the system and cause essential degradation due to ICI [12].

The uncertainty in the arrival time of the OFDM symbol is modelled as a delay in the channel impulse response $S(i-\delta i)$, where δi is the unknown time of arrival (TOA) of a symbol [7]. δi is assumed to be rounded off to integer multiples of the data sampling time that equals to $\Delta t/N$. As long as the OFDM data frame arrives within the Guard Interval, no ISI occurs. However, if a time offset appears in the alignment of the OFDM data frame due to the incorrect detection of the TOA, phase shifts appears to the subchannel data. The amount of phase shift caused by the time offset in each subchannel increases with the subchannel index as Equation **(3)**. In addition, the channel response and the additive channel noise distort the signal significantly. The channel output is a multiplication of the channel response H_k at each subcarrier of the OFDM signal. The channel response H_k can be considered as a complex constant within the duration of the OFDM symbol time if the symbol time is much smaller than the coherence time of the channel. The channel noise $w_{n,i}$ is assumed to be an additive white Gaussian noise (AWGN) with power spectral density of $N_o/2$. The distorted OFDM signal at the receiver contains the channel response, the additive channel noise, and the phase shift caused by the carrier frequency offset, and can be expressed as below.

$$\begin{aligned}\hat{s}_{n,i+\delta i} &= \left(\frac{1}{\sqrt{N}}\sum_{k=0}^{N-1} S_{n,k} H_k e^{j\frac{2\pi k(i+\delta i)}{N}}\right) + w_{n,i} \\ &= \left(\frac{1}{\sqrt{N}}\sum_{k=0}^{N-1} S_{n,k} H_k e^{j\frac{2\pi k i}{N}}\right)\cdot e^{j\frac{2\pi k \delta i}{N}} + w_{n,i}\end{aligned} \qquad \textbf{(3)}$$

In order to receive the OFDM signal correctly, detection and estimation of the

TOA is significant to align the OFDM data frame and set up the FFT-windows for detecting the OFDM data.

3.3 Carrier Frequency Offset

In a wireless system, the oscillator of the RF receiver may not be tuned exactly to the transmitting RF carrier frequency f_c. The tuned frequency of the receiver oscillator contains a small frequency error f_{off}, that is the carrier frequency offset. The carrier frequency offset introduces a phase shift equals $e^{j2\pi \cdot f_{off} \cdot t}$ after down-converting the received signal to the baseband OFDM signal. In a digital system, the phase shift can be expressed in term of time index by $e^{j2\pi \cdot f_{off} \cdot i \cdot \Delta t}$.

The distorted OFDM signal at the receiver contains the channel response, the additive channel noise, and the phase shift caused by the carrier frequency offset, and can be expressed as below.

$$\hat{s}_{n,i} = \left(\frac{1}{\sqrt{N}} \sum_{k=0}^{N-1} S_{n,k} H_k e^{j\frac{2\pi ki}{N}} \right) \cdot e^{j2\pi \cdot f_{off} \cdot i \cdot \Delta t} + w_{n,i} = \tilde{r}_{n,i} \cdot e^{j2\pi \cdot i \cdot \frac{f_{off}}{N \cdot \Delta f}} + w_{n,i} \qquad \textbf{(4)}$$

where $\tilde{r}_{n,i} = \frac{1}{\sqrt{N}} \sum_{k=0}^{N-1} S_{n,k} H_k e^{j\frac{2\pi ki}{N}}$ **(5)**

Assume the carrier frequency error equals a fraction of the frequency distance between subcarriers, i.e. $f_{off} = \delta k \cdot \Delta f$. Equation **(5)** is expressed in term of δk as below.

$$\hat{s}_{n,i} = \tilde{r}_{n,i} \cdot e^{j2\pi \cdot i \cdot \frac{\delta k \cdot \Delta f}{N \cdot \Delta f}} + w_{n,i} = \tilde{r}_{n,i} \cdot e^{j2\pi \cdot i \cdot \frac{\delta k}{N}} + w_{n,i} = \tilde{r}_{n,i} \cdot \gamma_i + w_{n,i} \qquad \textbf{(6)}$$

where $\gamma_i = e^{j\frac{2\pi \delta k i}{N}}$ **(7)**

The carrier frequency offset causes a phase rotation that is expressed in γ_i. Since γ_i is independent of k but dependent on i, the carrier frequency offset cannot be lumped into subchannel responses or removed after FFT during reception. However, we can estimate f_{off} in term of δk by introducing a training sequence in order to compensate the phase change of the OFDM signal to improve the reception of data frames.

When both time offset and carrier frequency offset appear in the OFDM system, the synchronization becomes a complicated problem.

$$\hat{s}_{n,i+\delta i} = \tilde{r}_{n,i+\delta i} \cdot e^{j2\pi\cdot(i+\delta i)\cdot\frac{\delta k}{N}} + w_{n,i+\delta i} = \left(\frac{1}{\sqrt{N}} \sum_{k=0}^{N-1} S_{n,k} H_k e^{j\frac{2\pi k(i+\delta i)}{N}} \right) \cdot e^{j2\pi\cdot(i+\delta i)\cdot\frac{\delta k}{N}} + w_{n,i+\delta i}$$

$$= \left(\frac{1}{\sqrt{N}} \sum_{k=0}^{N-1} S_{n,k} H_k e^{j\frac{2\pi ki}{N}} \cdot e^{j\frac{2\pi k\delta i}{N}} \cdot e^{j2\pi\cdot(i+\delta i)\cdot\frac{\delta k}{N}} \right) + w_{n,i+\delta i}$$

$$= \left(\frac{1}{\sqrt{N}} \sum_{k=0}^{N-1} S_{n,k} H_k e^{j\frac{2\pi ki}{N}} \cdot \vartheta_k \right) + w_{n,i+\delta i} \qquad \textbf{(8)}$$

where $\vartheta_k = e^{j\frac{2\pi k\delta i}{N}} \cdot e^{j2\pi\cdot(i+\delta i)\cdot\frac{\delta k}{N}}$ **(9)**

A synchronizer cannot distinguish between phase shifts introduced by the channel and those introduced by symbol time delays [7]. In order to tackle the problem, the frame alignment should be achieved before estimating the frequency offset.

4. SYNCHRONIZATION FOR 802.11A OFDM SYSTEMS

This project focuses on analyzing the structure of the PLCP "Short" and "Long" training symbols and researching methods to synchronize OFDM systems for indoor residential applications. In order to propose a robust system with a low BER, the major tasks to be resolved include the estimation of the symbol timing to determine the beginning of the symbol block, the estimation of the frame starting position, and the estimation of the carrier frequency offset.

The first task to do is analyzing the OFDM training structure that consists of 10 "Short" training symbols and 2 "Long" training symbols in order to understand their characteristics and usages as described in IEEE 802.11a standard.

4.1 "Short" Training Symbols [2]

A "Short" OFDM training symbol consists of 12 subcarriers, which are modulated by the elements of the sequence S, given by

$$S_{26,26} =$$
$$\sqrt{\tfrac{13}{6}} \cdot \{0,0,1+j,0,0,0,-1-j,0,0,0,1+j,0,0,0,-1-j,0,0,0,-1-j,0,0,0,1+j,$$
$$0,0,0,0,0,0,0,-1-j,0,0,0,-1-j,0,0,0,1+j,0,0,0,1+j,0,0,0,1+j,0,0,0,1+j,0,0\} \quad \textbf{(10)}$$

The multiplication factor of $\sqrt{\frac{13}{6}}$ is used to normalize the average power of the resulting OFDM symbol, which utilizes 12 out of 52 subcarriers. The 52 subcarriers plus a dc channel of the sequence S are mapped into the IFFT converter with a length of 64-sample inputs. After completing the IFFT conversion, the mapped sequence of S is

converted to a 64-sample sequence, which represents a single period, in time domain. The 64-sample sequence in time domain is extended periodically to a 161-sample sequence. Windowing is applied, by multiply 0.5 to the fist sample and the last sample of the extended sequence, to obtain the final extended sequence of 161 samples in time domain.

The final extended sequence, which is called "Short training sequence" in the following paragraphs, represents 10 "Short" symbols in total, and each symbol has 16 samples.

Table 1 shows the "Short training sequence" consists of 10 "Short" symbols, and the shaded data illustrates a single period of the IFFT conversion of the mapped sequence of S.

Symbol #1		Symbol #2		Symbol #3		Symbol #4		Symbol #5		Symbol #6	
#0-15		#16-31		#32-47		#48-63		#64-79		#80-95	
Real	Img	Real	Img	Real	Img	Real	Img	Real	Img	Real	Img
0.023	0.023	0.046	0.046	0.046	0.046	0.046	0.046	0.046	0.046	0.046	0.046
-0.132	0.002	-0.132	0.002	-0.132	0.002	-0.132	0.002	-0.132	0.002	-0.132	0.002
-0.013	-0.079	-0.013	-0.079	-0.013	-0.079	-0.013	-0.079	-0.013	-0.079	-0.013	-0.079
0.143	-0.013	0.143	-0.013	0.143	-0.013	0.143	-0.013	0.143	-0.013	0.143	-0.013
0.092	0.000	0.092	0.000	0.092	0.000	0.092	0.000	0.092	0.000	0.092	0.000
0.143	-0.013	0.143	-0.013	0.143	-0.013	0.143	-0.013	0.143	-0.013	0.143	-0.013
-0.013	-0.079	-0.013	-0.079	-0.013	-0.079	-0.013	-0.079	-0.013	-0.079	-0.013	-0.079
-0.132	0.002	-0.132	0.002	-0.132	0.002	-0.132	0.002	-0.132	0.002	-0.132	0.002
0.046	0.046	0.046	0.046	0.046	0.046	0.046	0.046	0.046	0.046	0.046	0.046
0.002	-0.132	0.002	-0.132	0.002	-0.132	0.002	-0.132	0.002	-0.132	0.002	-0.132
-0.079	-0.013	-0.079	-0.013	-0.079	-0.013	-0.079	-0.013	-0.079	-0.013	-0.079	-0.013
-0.013	0.143	-0.013	0.143	-0.013	0.143	-0.013	0.143	-0.013	0.143	-0.013	0.143
0.000	0.092	0.000	0.092	0.000	0.092	0.000	0.092	0.000	0.092	0.000	0.092
-0.013	0.143	-0.013	0.143	-0.013	0.143	-0.013	0.143	-0.013	0.143	-0.013	0.143
-0.079	-0.013	-0.079	-0.013	-0.079	-0.013	-0.079	-0.013	-0.079	-0.013	-0.079	-0.013
0.002	-0.132	0.002	-0.132	0.002	-0.132	0.002	-0.132	0.002	-0.132	0.002	-0.132

Symbol #7		Symbol #8		Symbol #9		Symbol #10			
#96-111		#112-127		#128-143		#144-159		#160	
Real	Img	Real	Img	Real	Img	Real	Img	Real	Img
0.046	0.046	0.046	0.046	0.046	0.046	0.046	0.046	0.023	0.023
-0.132	0.002	-0.132	0.002	-0.132	0.002	-0.132	0.002		
-0.013	-0.079	-0.013	-0.079	-0.013	-0.079	-0.013	-0.079		
0.143	-0.013	0.143	-0.013	0.143	-0.013	0.143	-0.013		
0.092	0.000	0.092	0.000	0.092	0.000	0.092	0.000		
0.143	-0.013	0.143	-0.013	0.143	-0.013	0.143	-0.013		
-0.013	-0.079	-0.013	-0.079	-0.013	-0.079	-0.013	-0.079		
-0.132	0.002	-0.132	0.002	-0.132	0.002	-0.132	0.002		
0.046	0.046	0.046	0.046	0.046	0.046	0.046	0.046		
0.002	-0.132	0.002	-0.132	0.002	-0.132	0.002	-0.132		
-0.079	-0.013	-0.079	-0.013	-0.079	-0.013	-0.079	-0.013		
-0.013	0.143	-0.013	0.143	-0.013	0.143	-0.013	0.143		
0.000	0.092	0.000	0.092	0.000	0.092	0.000	0.092		
-0.013	0.143	-0.013	0.143	-0.013	0.143	-0.013	0.143		
-0.079	-0.013	-0.079	-0.013	-0.079	-0.013	-0.079	-0.013		
0.002	-0.132	0.002	-0.132	0.002	-0.132	0.002	-0.132		

Table 1 –" Short Training Sequence" in Time Domain

The plots in Figure 4 and Figure 5 show the characteristics of the "Short" OFDM symbols in I-Q diagram, in time domain and in frequency domain. The "Short" OFDM symbols are BPSK data that have high peak-to-average power ratios (PAPR), but have rapid phase and amplitude changes in time domain. The 10 "Short" training symbols are made up of 16 samples per symbol in time domain. They are repeating themselves periodically every 16 samples spacing.

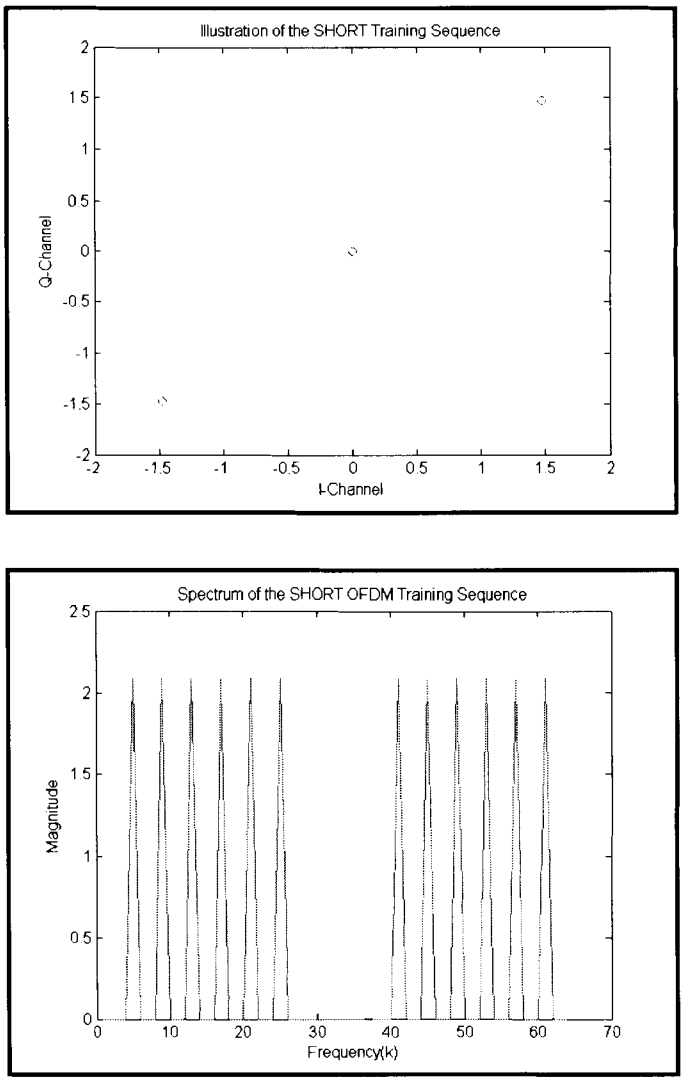

Figure 4 – "Short Training Sequence" in Frequency Domain

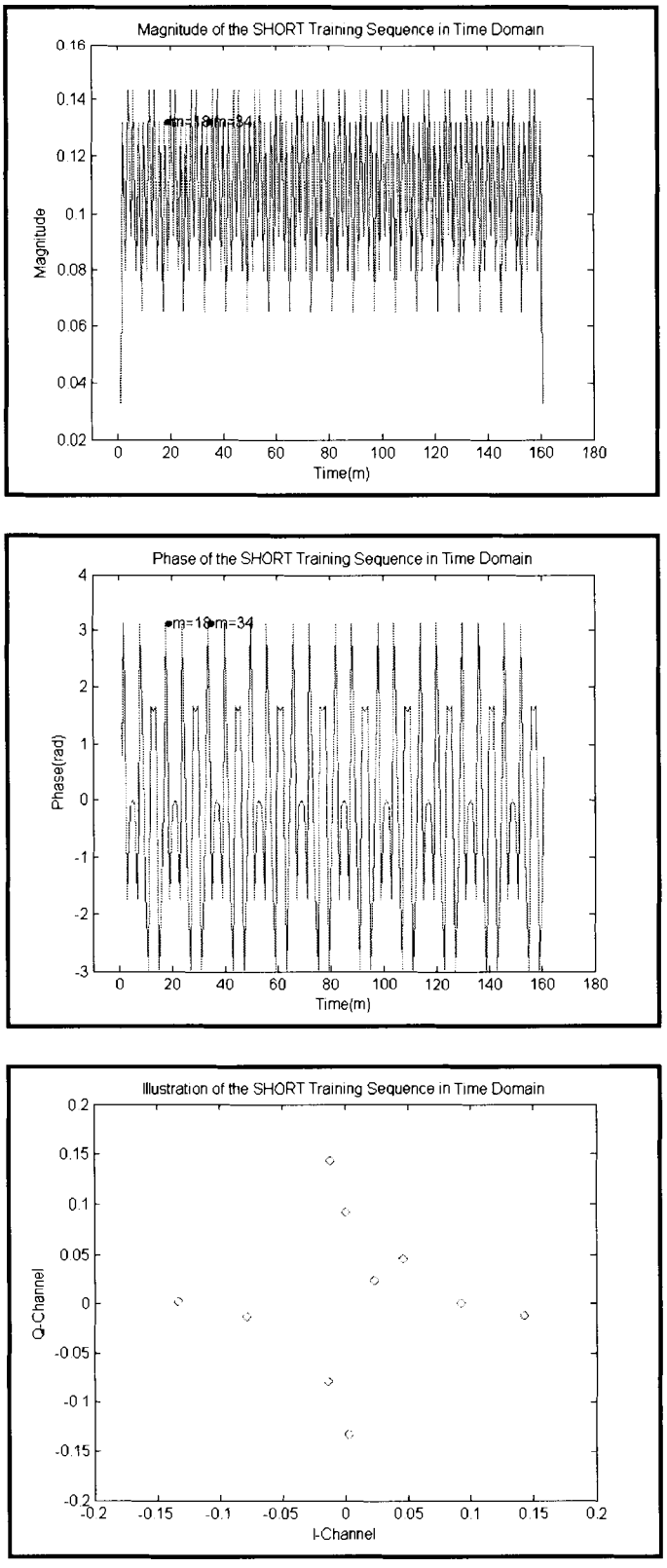

Figure 5 – "Short Training Sequence" in Time Domain

The "Short training sequence" has 10 repetitions in time domain samples and has a high PAPR in frequency domain samples. Therefore, it is possible to use time domain samples, or to use frequency domain samples, or to use both to look for an accurate time or frame synchronization. Non-coherent differential detection can be used to estimate CFO by forming the correlations with time domain samples.

4.2 "Long" Training Symbols [2]

A "Long" OFDM symbol consists of 53 subcarriers, which are modulated by the elements of the sequence $\mathcal{L}$, given by

$$\mathcal{L}_{26,26} =$$
$$\{1,1,-1,-1,1,1,\ -1,1,-1,1,1,1,1,1,1,-1,-1,1,1,-1,1,-1,1,1,1,1,1,0,$$
$$1,-1,-1,1,1,-1,1,-1,1,-1,-1,-1,-1,-1,1,1,-1,-1,1,-1,1,-1,1,1,1,1\} \quad \textbf{(11)}$$

The 52 subcarriers plus a dc channel of the sequence $\mathcal{L}$ are mapped into the IFFT converter with a length of 64-sample inputs. After completing the IFFT conversion, the mapped sequence of $\mathcal{L}$ is converted to a 64-sample sequence, which represents a single period, in time domain. The 64-sample sequence in time domain is extended periodically to a 161-sample sequence, which includes a 32-sample guard interval. The guard interval contains the last 32 samples of the single period sequence. Windowing is applied, by multiply 0.5 to the fist sample and the last sample of the extended sequence, to obtain the final extended sequence of 161 samples in time domain.

The final extended sequence, which is called "Long training sequence" in the following paragraphs, represents a 1.6 μs "Long" guard interval and 2 "Long" symbols.

Table 2 shows the "Long training sequence" consists of a 1.6 μs "Long" guard interval and 2 "Long" symbols, and the shaded data illustrates a single period of the IFFT conversion of the mapped sequence of $\mathcal{L}$.

Guard Interval				Symbol #1							
#0-15		#16-31		#32-47		#48-63		#64-79		#80-95	
Real	Img	Real	Img	Real	Img	Real	Img	Real	Img	Real	Img
-0.078	0.000	0.062	0.062	0.156	0.000	0.062	-0.062	-0.156	0.000	0.062	0.062
0.012	-0.098	0.119	0.004	-0.005	-0.120	0.037	0.098	0.012	-0.098	0.119	0.004
0.092	-0.106	-0.022	-0.161	0.040	-0.111	-0.057	0.039	0.092	-0.106	-0.022	-0.161
-0.092	-0.115	0.059	0.015	0.097	0.083	-0.131	0.065	-0.092	-0.115	0.059	0.015
-0.003	-0.054	0.024	0.059	0.021	0.028	0.082	0.092	-0.003	-0.054	0.024	0.059
0.075	0.074	-0.137	0.047	0.060	-0.088	0.070	0.014	0.075	0.074	-0.137	0.047
-0.127	0.021	0.001	0.115	-0.115	-0.055	-0.060	0.081	-0.127	0.021	0.001	0.115
-0.122	0.017	0.053	-0.004	-0.038	-0.106	-0.056	-0.022	-0.122	0.017	0.053	-0.004
-0.035	0.151	0.098	0.026	0.098	-0.026	-0.035	-0.151	-0.035	0.151	0.098	0.026
-0.056	0.022	-0.038	0.106	0.053	0.004	-0.122	-0.017	-0.056	0.022	-0.038	0.106
-0.060	-0.081	-0.115	0.055	0.001	-0.115	-0.127	-0.021	-0.060	-0.081	-0.115	0.055
0.070	-0.014	0.060	0.088	-0.137	-0.047	0.075	-0.074	0.070	-0.014	0.060	0.088
0.082	-0.092	0.021	-0.028	0.024	-0.059	-0.003	0.054	0.082	-0.092	0.021	-0.028
-0.131	-0.065	0.097	-0.083	0.059	-0.015	-0.092	0.115	-0.131	-0.065	0.097	-0.083
-0.057	-0.039	0.040	0.111	-0.022	0.161	0.092	0.106	-0.057	-0.039	0.040	0.111
0.037	-0.098	-0.005	0.120	0.119	-0.004	0.012	0.098	0.037	-0.098	-0.005	0.120
Symbol #2											
#96-111		#112-127		#128-143		#144-159		#160			
Real	Img	Real	Img	Real	Img	Real	Img	Real	Img		
0.156	0.000	0.062	-0.062	-0.156	0.000	0.062	0.062	0.078	0.000		
-0.005	-0.120	0.037	0.098	0.012	-0.098	0.119	0.004				
0.040	-0.111	-0.057	0.039	0.092	-0.106	-0.022	-0.161				
0.097	0.083	-0.131	0.065	-0.092	-0.115	0.059	0.015				
0.021	0.028	0.082	0.092	-0.003	-0.054	0.024	0.059				
0.060	-0.088	0.070	0.014	0.075	0.074	-0.137	0.047				
-0.115	-0.055	-0.060	0.081	-0.127	0.021	0.001	0.115				
-0.038	-0.106	-0.056	-0.022	-0.122	0.017	0.053	-0.004				
0.098	-0.026	-0.035	-0.151	-0.035	0.151	0.098	0.026				
0.053	0.004	-0.122	-0.017	-0.056	0.022	-0.038	0.106				
0.001	-0.115	-0.127	-0.021	-0.060	-0.081	-0.115	0.055				
-0.137	-0.047	0.075	-0.074	0.070	-0.014	0.060	0.088				
0.024	-0.059	-0.003	0.054	0.082	-0.092	0.021	-0.028				
0.059	-0.015	-0.092	0.115	-0.131	-0.065	0.097	-0.083				
-0.022	0.161	0.092	0.106	-0.057	-0.039	0.040	0.111				
0.119	-0.004	0.012	0.098	0.037	-0.098	-0.005	0.120				

Table 2 – "Long Training Sequence" in Time Domain

The plots in Figure 6 and Figure 7 show the characteristics of the "Long" training symbols in I-Q diagram, in time domain and in frequency domain. The "Long" OFDM symbols are BPSK data that change slowly in phase compared to the "Short" training symbols, but change rapidly in amplitude in time domain. The "Long" training symbols are made up of two symbols of 64 samples, repeating themselves periodically every 64 samples spacing. Since 52 subcarriers contain data compared to 12 subcarriers in the "Short" symbols, using "Long" training symbols is expected to have a better estimation of carrier frequency offset.

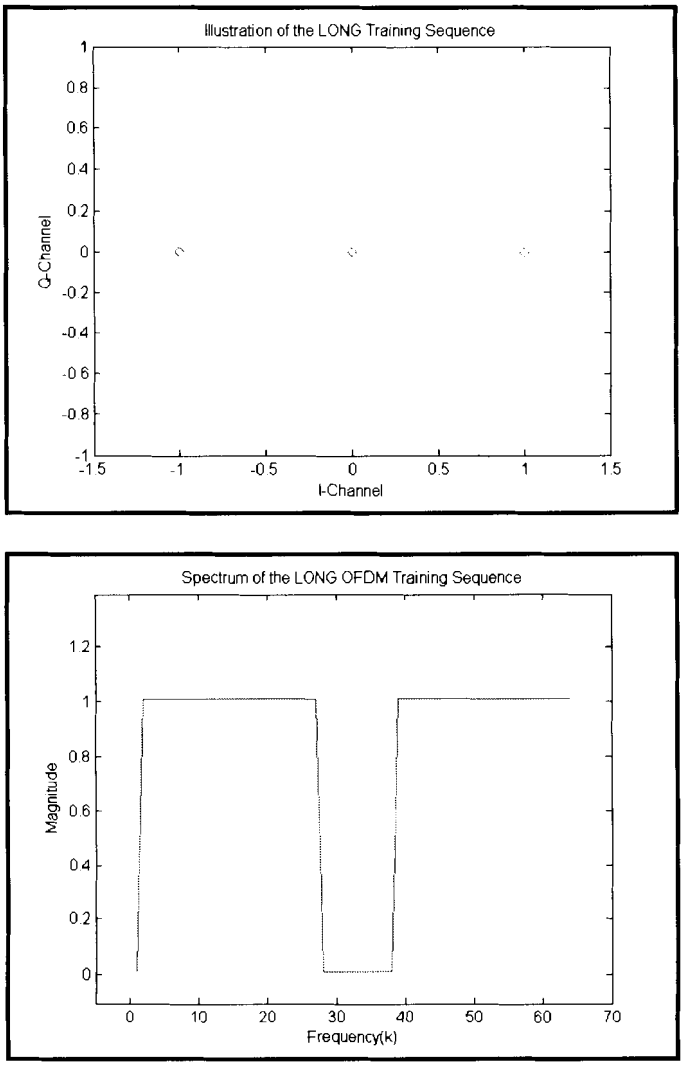

Figure 6 – "Long Training Sequence" in Frequency Domain

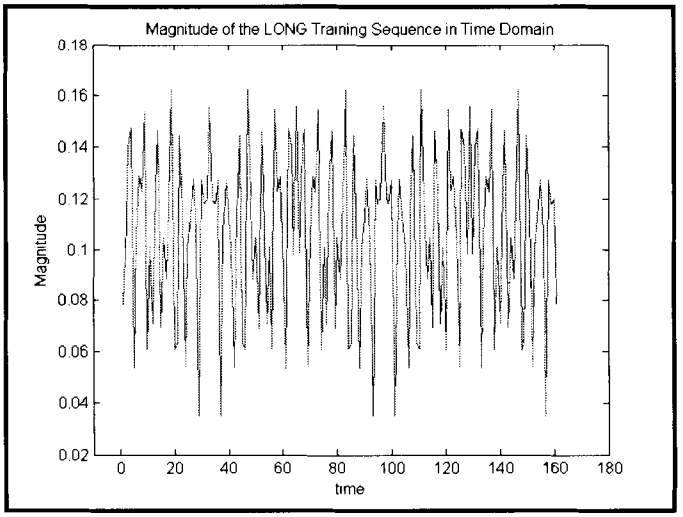

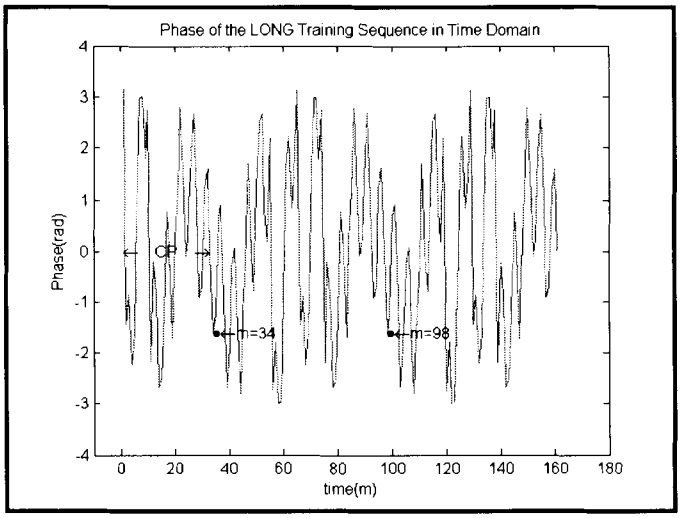

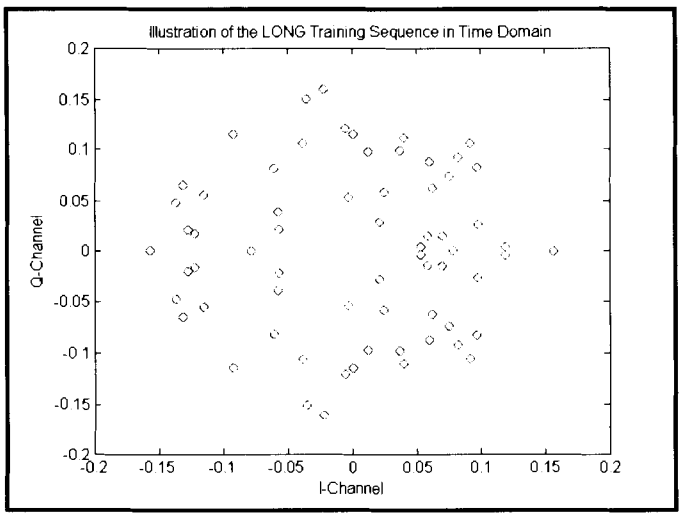

Figure 7 – "Long Training Sequence" in Time Domain

5. PROPOSED SYNCHRONIZATION METHODS

5.1 Time/Frame Synchronization

The time/frame synchronization process consists of two steps including acquisition and time tracking. Acquisition is the first step to determine the existence of the "Short" symbols by searching for periodic structure within the OFDM signal [12]. Time domain information should be used for fast and reliable acquisition. After knowing that the "Short" symbols appear, the next step is time tracking that accomplishes the data frame alignment by estimating the time offset error and the actual time of arrival of the OFDM data frame. The carrier frequency offset is unknown during the frame synchronization.

The Mean Square Error (MSE) approach described in [12] can be applied similarly for detecting the TOA of the "Short" symbols. A periodicity metric is defined as below.

$$M_p(\delta i) = \sum_{i=0}^{W-1} \left| \hat{s}(i+\delta i+L_S) - \hat{s}(i+\delta i) \right|^2 \qquad \textbf{(12)}$$

where W is the length of observation window which is chosen to cover the length of the 10 "Short" symbols, L_s is the length of each "Short" symbol, and δi is the unknown time offset. The metric computes the MSE between two "Short" symbols separated by the length of 16 samples.

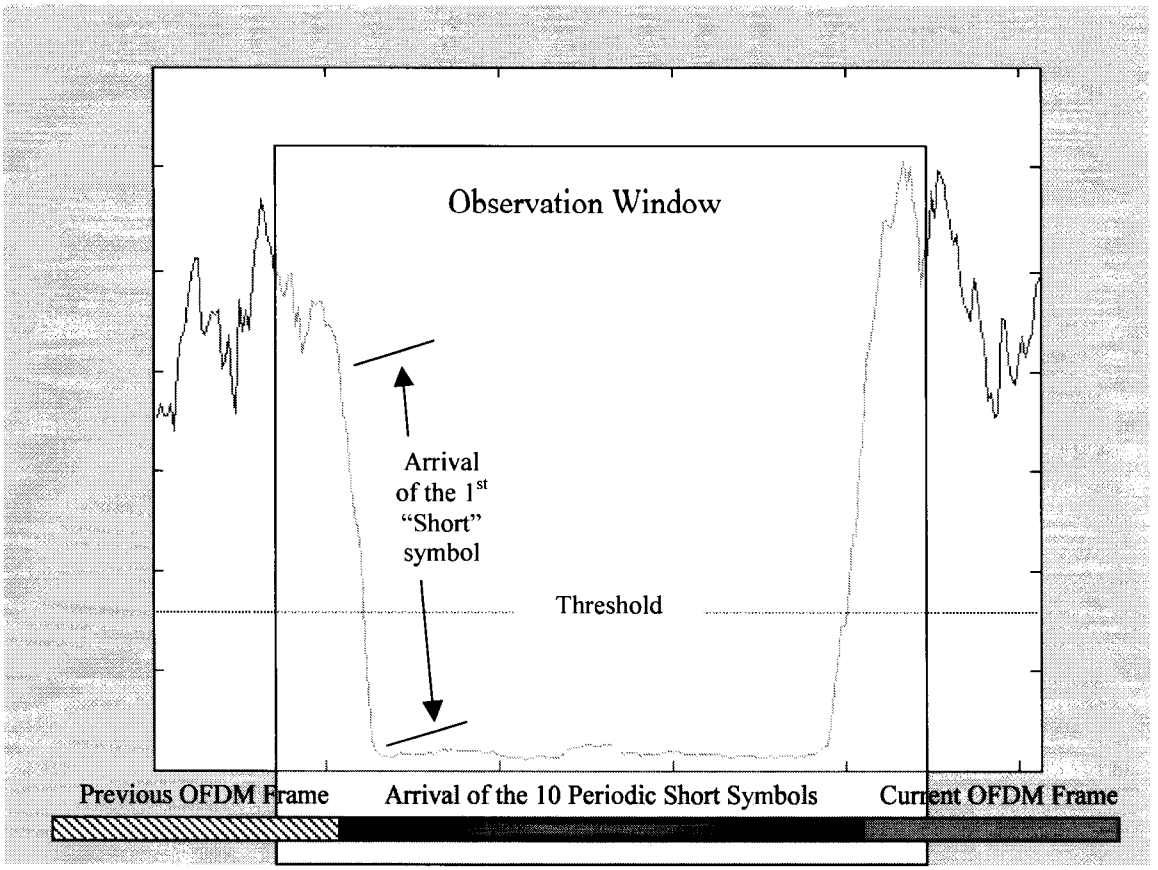

Figure 8 – Periodicity Metric for Detecting the Arrival of 10 "Short" Symbols

Mininizing the periodicity metric in **(12)** leads to an estimate for the right position of the FFT window [12].

$$\underset{\delta i}{Min}\{M_p(\delta i)\} \rightarrow \hat{\delta i} \qquad \textbf{(13)}$$

Referring to the Figure 8, the periodic structure of the OFDM signal presents when there is a minimum region in the periodicity metric. Since the "Short" symbols are periodic, the minimum region of the metric can identify the presence of the "Short" symbols.

5.1.1 Acquisition

When the OFDM data stream goes into the receiver, the periodicity metric is computed and monitored. During the stage of acquisition, the periodicity metric is used to identify the presence of the periodic signal if the periodicity metric shows a minimum region. Graphically, the minimum region can be easily identified; however, the task is difficult to be achieved quantitatively when the noises present. A threshold comparison is applied to determine the minimum region appears in the periodicity metric. The choice of the threshold is critical to the result under a noisy system. Since the minimum region of the periodicity metric varies depending on the signal strength, an absolute threshold is inappropriate. Therefore, a proposed solution is choosing the threshold with reference to the max range of the periodicity metric during the observation window. The max range is defined as the range between the maximum and the minimum of the periodicity metric.

Referring to the Figure 8, the slope region at the left indicates the periodic signal, the first 16-sample "Short" symbol, is arriving. The lower portion of the slope contains a higher certainty of the arrival of the first symbol. Therefore, the threshold is better to be chosen at the lower portion of the slope, that is the time region when a half of the first "Short" symbol has arrived. After finding the first location of the first "Short" symbol drops below the threshold, the receiver keeps monitoring the following 16 samples if they are below the threshold. If there is a region consecutively below the threshold for a length equal to or longer than a single "Short" symbol, the presence of the two "Short" symbols is assumed. In order to confirm the arrival of the "Short" symbols, the receiver takes a FFT conversion using the 64 received time domain samples to validate the result. To avoid the uncertainty of the start of the minimum region in the periodicity metric, the

FFT window is set at 16 samples after the first location drops below the threshold, that is within the arrival time of the second "Short" symbol. Once the "Short" symbols are recognized with the metric, tracking the time offset of the actual TOA of the first "Short" symbol will be the next step for the time/frame synchronization.

5.1.2 Tracking

Since the FFT window is randomly picked by the threshold comparison, the absolute time of the start of the FFT window should be determined in order to estimate the TOA and align the OFDM frame properly. The time offset creates phase shifts or rotations of the frequency domain data. By studying the shifts of the frequency domain data, the start of the FFT window can be found corresponding to the 16 time slots of one "Short" symbol. The absolute time of the FFT window can be determined since the window starts within the second "Short" symbol. A look-up table easily accomplishes the task. Taking a 64-sample FFT conversion of an expected "Short" Symbol with rotating the start of the FFT window creates the look-up table in Table 3. Minimum MSE detection is used to determine the best match of the look-up table as follow.

$$MSE = \sum_{i=0}^{N-1} \left| \hat{S}_{n,i} - S_{n,i} \right|^2 \qquad \textbf{(14)}$$

Once the absolute time of the FFT window is determined, the TOA can be estimated accordingly, that is 16 time slots before the start of the FFT window.

Data #	Start at 1st Position	Start at 2nd Position	Start at 3rd Position	Start at 4th Position	Start at 5th Position	Start at 6th Position
1	-0.0230 - 0.0230i	-0.0230 - 0.0230i	-0.0230 - 0.0230i	-0.0230 - 0.0230i	-0.0230 - 0.0230i	-0.0230 - 0.0230i
2	-0.0230 - 0.0230i	-0.0206 - 0.0251i	-0.0181 - 0.0270i	-0.0153 - 0.0287i	-0.0124 - 0.0301i	-0.0094 - 0.0311i
3	-0.0230 - 0.0230i	-0.0181 - 0.0270i	-0.0124 - 0.0301i	-0.0063 - 0.0319i	0 - 0.0325i	0.0063 - 0.0319i
4	-0.0230 - 0.0230i	-0.0153 - 0.0287i	-0.0063 - 0.0319i	0.0032 - 0.0324i	0.0124 - 0.0301i	0.0206 - 0.0251i
5	-1.4950 - 1.4950i	-0.8091 - 1.9533i	-0.0000 - 2.1142i	0.8091 - 1.9533i	1.4950 - 1.4950i	1.9533 - 0.8091i
6	-0.0230 - 0.0230i	-0.0094 - 0.0311i	0.0063 - 0.0319i	0.0206 - 0.0251i	0.0301 - 0.0124i	0.0324 + 0.0032i
7	-0.0230 - 0.0230i	-0.0063 - 0.0319i	0.0124 - 0.0301i	0.0270 - 0.0181i	0.033	0.0270 + 0.0181i
8	-0.0230 - 0.0230i	-0.0032 - 0.0324i	0.0181 - 0.0270i	0.0311 - 0.0094i	0.0301 + 0.0124i	0.0153 + 0.0287i
9	-1.4950 - 1.4950i	0.0000 - 2.1142i	1.4950 - 1.4950i	2.1142 + 0.0000i	1.4950 + 1.4950i	-0.0000 + 2.1142i
10	-0.0230 - 0.0230i	0.0032 - 0.0324i	0.0270 - 0.0181i	0.0311 + 0.0094i	0.0124 + 0.0301i	-0.0153 + 0.0287i
11	-0.0230 - 0.0230i	0.0063 - 0.0319i	0.0301 - 0.0124i	0.0270 + 0.0181i	0 + 0.0325i	-0.0270 + 0.0181i
12	-0.0230 - 0.0230i	0.0094 - 0.0311i	0.0319 - 0.0063i	0.0206 + 0.0251i	-0.0124 + 0.0301i	-0.0324 + 0.0032i
13	1.4490 + 1.4490i	-0.7842 + 1.8932i	-2.0491 - 0.0000i	-0.7842 - 1.8932i	1.4490 - 1.4490i	1.8932 + 0.7842i
14	-0.0230 - 0.0230i	0.0153 - 0.0287i	0.0319 + 0.0063i	0.0032 + 0.0324i	-0.0301 + 0.0124i	-0.0206 - 0.0251i
15	-0.0230 - 0.0230i	0.0181 - 0.0270i	0.0301 + 0.0124i	-0.0063 + 0.0319i	-0.033	-0.0063 - 0.0319i
16	-0.0230 - 0.0230i	0.0206 - 0.0251i	0.0270 + 0.0181i	-0.0153 + 0.0287i	-0.0301 - 0.0124i	0.0094 - 0.0311i
17	1.4490 + 1.4490i	-1.4490 + 1.4490i	-1.4490 - 1.4490i	1.4490 - 1.4490i	1.4490 + 1.4490i	-1.4490 + 1.4490i
18	-0.0230 - 0.0230i	0.0251 - 0.0206i	0.0181 + 0.0270i	-0.0287 + 0.0153i	-0.0124 - 0.0301i	0.0311 - 0.0094i
19	-0.0230 - 0.0230i	0.0270 - 0.0181i	0.0124 + 0.0301i	-0.0319 + 0.0063i	0 - 0.0325i	0.0319 + 0.0063i
20	-0.0230 - 0.0230i	0.0287 - 0.0153i	0.0063 + 0.0319i	-0.0324 - 0.0032i	0.0124 - 0.0301i	0.0251 + 0.0206i
21	1.4490 + 1.4490i	-1.8932 + 0.7842i	0.0000 - 2.0491i	1.8932 + 0.7842i	-1.4490 + 1.4490i	-0.7842 - 1.8932i
22	-0.0230 - 0.0230i	0.0311 - 0.0094i	-0.0063 + 0.0319i	-0.0251 - 0.0206i	0.0301 - 0.0124i	-0.0032 + 0.0324i
23	-0.0230 - 0.0230i	0.0319 - 0.0063i	-0.0124 + 0.0301i	-0.0181 - 0.0270i	0.033	-0.0181 + 0.0270i
24	-0.0230 - 0.0230i	0.0324 - 0.0032i	-0.0181 + 0.0270i	-0.0094 - 0.0311i	0.0301 + 0.0124i	-0.0287 + 0.0153i
25	1.4490 + 1.4490i	-2.0491 + 0.0000i	1.4490 - 1.4490i	0.0000 + 2.0491i	-1.4490 - 1.4490i	2.0491 - 0.0000i
26	-0.0230 - 0.0230i	0.0324 + 0.0032i	-0.0270 + 0.0181i	0.0094 - 0.0311i	0.0124 + 0.0301i	-0.0287 - 0.0153i
27	-0.0230 - 0.0230i	0.0319 + 0.0063i	-0.0301 + 0.0124i	0.0181 - 0.0270i	0 + 0.0325i	-0.0181 - 0.0270i
28	-0.0230 - 0.0230i	0.0311 + 0.0094i	-0.0319 + 0.0063i	0.0251 - 0.0206i	-0.0124 + 0.0301i	-0.0032 - 0.0324i
29	-0.0230 - 0.0230i	0.0301 + 0.0124i	-0.0325 - 0.0000i	0.0301 - 0.0124i	-0.0230 + 0.0230i	0.0124 - 0.0301i
30	-0.0230 - 0.0230i	0.0287 + 0.0153i	-0.0319 - 0.0063i	0.0324 - 0.0032i	-0.0301 + 0.0124i	0.0251 - 0.0206i
31	-0.0230 - 0.0230i	0.0270 + 0.0181i	-0.0301 - 0.0124i	0.0319 + 0.0063i	-0.033	0.0319 - 0.0063i
32	-0.0230 - 0.0230i	0.0251 + 0.0206i	-0.0270 - 0.0181i	0.0287 + 0.0153i	-0.0301 - 0.0124i	0.0311 + 0.0094i

Table 3 – The Look-up Table for Tracking

Data #	Start at 1st Position	Start at 2nd Position	Start at 3rd Position	Start at 4th Position	Start at 5th Position	Start at 6th Position
33	-0.0230 - 0.0230i	0.0230 + 0.0230i	-0.0230 - 0.0230i	0.0230 + 0.0230i	-0.0230 - 0.0230i	0.0230 + 0.0230i
34	-0.0230 - 0.0230i	0.0206 + 0.0251i	-0.0181 - 0.0270i	0.0153 + 0.0287i	-0.0124 - 0.0301i	0.0094 + 0.0311i
35	-0.0230 - 0.0230i	0.0181 + 0.0270i	-0.0124 - 0.0301i	0.0063 + 0.0319i	0 - 0.0325i	-0.0063 + 0.0319i
36	-0.0230 - 0.0230i	0.0153 + 0.0287i	-0.0063 - 0.0319i	-0.0032 + 0.0324i	0.0124 - 0.0301i	-0.0206 + 0.0251i
37	-0.0230 - 0.0230i	0.0124 + 0.0301i	0.0000 - 0.0325i	-0.0124 + 0.0301i	0.0230 - 0.0230i	-0.0301 + 0.0124i
38	-0.0230 - 0.0230i	0.0094 + 0.0311i	0.0063 - 0.0319i	-0.0206 + 0.0251i	0.0301 - 0.0124i	-0.0324 - 0.0032i
39	-0.0230 - 0.0230i	0.0063 + 0.0319i	0.0124 - 0.0301i	-0.0270 + 0.0181i	0.033	-0.0270 - 0.0181i
40	-0.0230 - 0.0230i	0.0032 + 0.0324i	0.0181 - 0.0270i	-0.0311 + 0.0094i	0.0301 + 0.0124i	-0.0153 - 0.0287i
41	1.4490 + 1.4490i	-0.0000 - 2.0491i	-1.4490 + 1.4490i	2.0491 - 0.0000i	-1.4490 - 1.4490i	0.0000 + 2.0491i
42	-0.0230 - 0.0230i	-0.0032 + 0.0324i	0.0270 - 0.0181i	-0.0311 - 0.0094i	0.0124 + 0.0301i	0.0153 - 0.0287i
43	-0.0230 - 0.0230i	-0.0063 + 0.0319i	0.0301 - 0.0124i	-0.0270 - 0.0181i	0 + 0.0325i	0.0270 - 0.0181i
44	-0.0230 - 0.0230i	-0.0094 + 0.0311i	0.0319 - 0.0063i	-0.0206 - 0.0251i	-0.0124 + 0.0301i	0.0324 - 0.0032i
45	-1.4950 - 1.4950i	-0.8091 + 1.9533i	2.1142 + 0.0000i	-0.8091 - 1.9533i	-1.4950 + 1.4950i	1.9533 + 0.8091i
46	-0.0230 - 0.0230i	-0.0153 + 0.0287i	0.0319 + 0.0063i	-0.0032 - 0.0324i	-0.0301 + 0.0124i	0.0206 + 0.0251i
47	-0.0230 - 0.0230i	-0.0181 + 0.0270i	0.0301 + 0.0124i	0.0063 - 0.0319i	-0.033	0.0063 + 0.0319i
48	-0.0230 - 0.0230i	-0.0206 + 0.0251i	0.0270 + 0.0181i	0.0153 - 0.0287i	-0.0301 - 0.0124i	-0.0094 + 0.0311i
49	1.4490 + 1.4490i	1.4490 - 1.4490i	-1.4490 - 1.4490i	-1.4490 + 1.4490i	1.4490 + 1.4490i	1.4490 - 1.4490i
50	-0.0230 - 0.0230i	-0.0251 + 0.0206i	0.0181 + 0.0270i	0.0287 - 0.0153i	-0.0124 - 0.0301i	-0.0311 + 0.0094i
51	-0.0230 - 0.0230i	-0.0270 + 0.0181i	0.0124 + 0.0301i	0.0319 - 0.0063i	0 - 0.0325i	-0.0319 - 0.0063i
52	-0.0230 - 0.0230i	-0.0287 + 0.0153i	0.0063 + 0.0319i	0.0324 + 0.0032i	0.0124 - 0.0301i	-0.0251 - 0.0206i
53	-1.4950 - 1.4950i	-1.9533 + 0.8091i	-0.0000 + 2.1142i	1.9533 + 0.8091i	1.4950 - 1.4950i	-0.8091 - 1.9533i
54	-0.0230 - 0.0230i	-0.0311 + 0.0094i	-0.0063 + 0.0319i	0.0251 + 0.0206i	0.0301 - 0.0124i	0.0032 - 0.0324i
55	-0.0230 - 0.0230i	-0.0319 + 0.0063i	-0.0124 + 0.0301i	0.0181 + 0.0270i	0.033	0.0181 - 0.0270i
56	-0.0230 - 0.0230i	-0.0324 + 0.0032i	-0.0181 + 0.0270i	0.0094 + 0.0311i	0.0301 + 0.0124i	0.0287 - 0.0153i
57	-1.4950 - 1.4950i	-2.1142 - 0.0000i	-1.4950 + 1.4950i	-0.0000 + 2.1142i	1.4950 + 1.4950i	2.1142 + 0.0000i
58	-0.0230 - 0.0230i	-0.0324 - 0.0032i	-0.0270 + 0.0181i	-0.0094 + 0.0311i	0.0124 + 0.0301i	0.0287 + 0.0153i
59	-0.0230 - 0.0230i	-0.0319 - 0.0063i	-0.0301 + 0.0124i	-0.0181 + 0.0270i	0 + 0.0325i	0.0181 + 0.0270i
60	-0.0230 - 0.0230i	-0.0311 - 0.0094i	-0.0319 + 0.0063i	-0.0251 + 0.0206i	-0.0124 + 0.0301i	0.0032 + 0.0324i
61	1.4490 + 1.4490i	1.8932 + 0.7842i	2.0491 + 0.0000i	1.8932 - 0.7842i	1.4490 - 1.4490i	0.7842 - 1.8932i
62	-0.0230 - 0.0230i	-0.0287 - 0.0153i	-0.0319 - 0.0063i	-0.0324 + 0.0032i	-0.0301 + 0.0124i	-0.0251 + 0.0206i
63	-0.0230 - 0.0230i	-0.0270 - 0.0181i	-0.0301 - 0.0124i	-0.0319 - 0.0063i	-0.033	-0.0319 + 0.0063i
64	-0.0230 - 0.0230i	-0.0251 - 0.0206i	-0.0270 - 0.0181i	-0.0287 - 0.0153i	-0.0301 - 0.0124i	-0.0311 - 0.0094i

Table 3 – The Look-up Table for Tracking (Continued)

Data #	Start at 7th Position	Start at 8th Position	Start at 9th Position	Start at 10th Position	Start at 11th Position	Start at 12th Position
1	-0.0230 - 0.0230i	-0.0230 - 0.0230i	-0.0230 - 0.0230i	-0.0230 - 0.0230i	-0.0230 - 0.0230i	-0.0230 - 0.0230i
2	-0.0063 - 0.0319i	-0.0032 - 0.0324i	0 - 0.0325i	0.0032 - 0.0324i	0.0063 - 0.0319i	0.0094 - 0.0311i
3	0.0124 - 0.0301i	0.0181 - 0.0270i	0.0230 - 0.0230i	0.0270 - 0.0181i	0.0301 - 0.0124i	0.0319 - 0.0063i
4	0.0270 - 0.0181i	0.0311 - 0.0094i	0.033	0.0311 + 0.0094i	0.0270 + 0.0181i	0.0206 + 0.0251i
5	2.1142 - 0.0000i	1.9533 + 0.8091i	1.4950 + 1.4950i	0.8091 + 1.9533i	0.0000 + 2.1142i	-0.8091 + 1.9533i
6	0.0270 + 0.0181i	0.0153 + 0.0287i	0 + 0.0325i	-0.0153 + 0.0287i	-0.0270 + 0.0181i	-0.0324 + 0.0032i
7	0.0124 + 0.0301i	-0.0063 + 0.0319i	-0.0230 + 0.0230i	-0.0319 + 0.0063i	-0.0301 - 0.0124i	-0.0181 - 0.0270i
8	-0.0063 + 0.0319i	-0.0251 + 0.0206i	-0.033	-0.0251 - 0.0206i	-0.0063 - 0.0319i	0.0153 - 0.0287i
9	-1.4950 + 1.4950i	-2.1142 - 0.0000i	-1.4950 - 1.4950i	0.0000 - 2.1142i	1.4950 - 1.4950i	2.1142 + 0.0000i
10	-0.0319 + 0.0063i	-0.0251 - 0.0206i	0 - 0.0325i	0.0251 - 0.0206i	0.0319 + 0.0063i	0.0153 + 0.0287i
11	-0.0301 - 0.0124i	-0.0063 - 0.0319i	0.0230 - 0.0230i	0.0319 + 0.0063i	0.0124 + 0.0301i	-0.0181 + 0.0270i
12	-0.0181 - 0.0270i	0.0153 - 0.0287i	0.033	0.0153 + 0.0287i	-0.0181 + 0.0270i	-0.0324 - 0.0032i
13	-0.0000 + 2.0491i	-1.8932 + 0.7842i	-1.4490 - 1.4490i	0.7842 - 1.8932i	2.0491 + 0.0000i	0.7842 + 1.8932i
14	0.0181 - 0.0270i	0.0311 + 0.0094i	0 + 0.0325i	-0.0311 + 0.0094i	-0.0181 - 0.0270i	0.0206 - 0.0251i
15	0.0301 - 0.0124i	0.0181 + 0.0270i	-0.0230 + 0.0230i	-0.0270 - 0.0181i	0.0124 - 0.0301i	0.0319 + 0.0063i
16	0.0319 + 0.0063i	-0.0032 + 0.0324i	-0.033	-0.0032 - 0.0324i	0.0319 - 0.0063i	0.0094 + 0.0311i
17	-1.4490 - 1.4490i	1.4490 - 1.4490i	1.4490 + 1.4490i	-1.4490 + 1.4490i	-1.4490 - 1.4490i	1.4490 - 1.4490i
18	0.0063 + 0.0319i	-0.0324 + 0.0032i	0 - 0.0325i	0.0324 + 0.0032i	-0.0063 + 0.0319i	-0.0311 - 0.0094i
19	-0.0124 + 0.0301i	-0.0270 - 0.0181i	0.0230 - 0.0230i	0.0181 + 0.0270i	-0.0301 + 0.0124i	-0.0063 - 0.0319i
20	-0.0270 + 0.0181i	-0.0094 - 0.0311i	0.033	-0.0094 + 0.0311i	-0.0270 - 0.0181i	0.0251 - 0.0206i
21	2.0491 + 0.0000i	-0.7842 + 1.8932i	-1.4490 - 1.4490i	1.8932 - 0.7842i	-0.0000 + 2.0491i	-1.8932 - 0.7842i
22	-0.0270 - 0.0181i	0.0287 - 0.0153i	0 + 0.0325i	-0.0287 - 0.0153i	0.0270 - 0.0181i	0.0032 + 0.0324i
23	-0.0124 - 0.0301i	0.0319 + 0.0063i	-0.0230 + 0.0230i	-0.0063 - 0.0319i	0.0301 + 0.0124i	-0.0270 + 0.0181i
24	0.0063 - 0.0319i	0.0206 + 0.0251i	-0.033	0.0206 - 0.0251i	0.0063 + 0.0319i	-0.0287 - 0.0153i
25	-1.4490 + 1.4490i	-0.0000 - 2.0491i	1.4490 + 1.4490i	-2.0491 + 0.0000i	1.4490 - 1.4490i	0.0000 + 2.0491i
26	0.0319 - 0.0063i	-0.0206 + 0.0251i	0 - 0.0325i	0.0206 + 0.0251i	-0.0319 - 0.0063i	0.0287 - 0.0153i
27	0.0301 + 0.0124i	-0.0319 + 0.0063i	0.0230 - 0.0230i	-0.0063 + 0.0319i	-0.0124 - 0.0301i	0.0270 + 0.0181i
28	0.0181 + 0.0270i	-0.0287 - 0.0153i	0.033	-0.0287 + 0.0153i	0.0181 - 0.0270i	-0.0032 + 0.0324i
29	-0.0000 + 0.0325i	-0.0124 - 0.0301i	0.0230 + 0.0230i	-0.0301 - 0.0124i	0.0325 + 0.0000i	-0.0301 + 0.0124i
30	-0.0181 + 0.0270i	0.0094 - 0.0311i	0 + 0.0325i	-0.0094 - 0.0311i	0.0181 + 0.0270i	-0.0251 - 0.0206i
31	-0.0301 + 0.0124i	0.0270 - 0.0181i	-0.0230 + 0.0230i	0.0181 - 0.0270i	-0.0124 + 0.0301i	0.0063 - 0.0319i
32	-0.0319 - 0.0063i	0.0324 + 0.0032i	-0.033	0.0324 - 0.0032i	-0.0319 + 0.0063i	0.0311 - 0.0094i

Table 3 – The Look-up Table for Tracking (Continued)

Data #	Start at 7th Position	Start at 8th Position	Start at 9th Position	Start at 10th Position	Start at 11th Position	Start at 12th Position
33	-0.0230 - 0.0230i	0.0230 + 0.0230i	-0.0230 - 0.0230i	0.0230 + 0.0230i	-0.0230 - 0.0230i	0.0230 + 0.0230i
34	-0.0063 - 0.0319i	0.0032 + 0.0324i	0 - 0.0325i	-0.0032 + 0.0324i	0.0063 - 0.0319i	-0.0094 + 0.0311i
35	0.0124 - 0.0301i	-0.0181 + 0.0270i	0.0230 - 0.0230i	-0.0270 + 0.0181i	0.0301 - 0.0124i	-0.0319 + 0.0063i
36	0.0270 - 0.0181i	-0.0311 + 0.0094i	0.033	-0.0311 - 0.0094i	0.0270 + 0.0181i	-0.0206 - 0.0251i
37	0.0325 + 0.0000i	-0.0301 - 0.0124i	0.0230 + 0.0230i	-0.0124 - 0.0301i	-0.0000 + 0.0325i	0.0124 - 0.0301i
38	0.0270 + 0.0181i	-0.0153 - 0.0287i	0 + 0.0325i	0.0153 - 0.0287i	-0.0270 + 0.0181i	0.0324 - 0.0032i
39	0.0124 + 0.0301i	0.0063 - 0.0319i	-0.0230 + 0.0230i	0.0319 - 0.0063i	-0.0301 - 0.0124i	0.0181 + 0.0270i
40	-0.0063 + 0.0319i	0.0251 - 0.0206i	-0.033	0.0251 + 0.0206i	-0.0063 - 0.0319i	-0.0153 + 0.0287i
41	1.4490 - 1.4490i	-2.0491 + 0.0000i	1.4490 + 1.4490i	-0.0000 - 2.0491i	-1.4490 + 1.4490i	2.0491 - 0.0000i
42	-0.0319 + 0.0063i	0.0251 + 0.0206i	0 - 0.0325i	-0.0251 + 0.0206i	0.0319 + 0.0063i	-0.0153 - 0.0287i
43	-0.0301 - 0.0124i	0.0063 + 0.0319i	0.0230 - 0.0230i	-0.0319 - 0.0063i	0.0124 + 0.0301i	0.0181 - 0.0270i
44	-0.0181 - 0.0270i	-0.0153 + 0.0287i	0.033	-0.0153 - 0.0287i	-0.0181 + 0.0270i	0.0324 + 0.0032i
45	0.0000 - 2.1142i	-1.9533 + 0.8091i	1.4950 + 1.4950i	0.8091 - 1.9533i	-2.1142 - 0.0000i	0.8091 + 1.9533i
46	0.0181 - 0.0270i	-0.0311 - 0.0094i	0 + 0.0325i	0.0311 - 0.0094i	-0.0181 - 0.0270i	-0.0206 + 0.0251i
47	0.0301 - 0.0124i	-0.0181 - 0.0270i	-0.0230 + 0.0230i	0.0270 + 0.0181i	0.0124 - 0.0301i	-0.0319 - 0.0063i
48	0.0319 + 0.0063i	0.0032 - 0.0324i	-0.033	0.0032 + 0.0324i	0.0319 - 0.0063i	-0.0094 - 0.0311i
49	-1.4490 - 1.4490i	-1.4490 + 1.4490i	1.4490 + 1.4490i	1.4490 - 1.4490i	-1.4490 - 1.4490i	-1.4490 + 1.4490i
50	0.0063 + 0.0319i	0.0324 - 0.0032i	0 - 0.0325i	-0.0324 - 0.0032i	-0.0063 + 0.0319i	0.0311 + 0.0094i
51	-0.0124 + 0.0301i	0.0270 + 0.0181i	0.0230 - 0.0230i	-0.0181 - 0.0270i	-0.0301 + 0.0124i	0.0063 + 0.0319i
52	-0.0270 + 0.0181i	0.0094 + 0.0311i	0.033	0.0094 - 0.0311i	-0.0270 - 0.0181i	-0.0251 + 0.0206i
53	-2.1142 - 0.0000i	-0.8091 + 1.9533i	1.4950 + 1.4950i	1.9533 - 0.8091i	0.0000 - 2.1142i	-1.9533 - 0.8091i
54	-0.0270 - 0.0181i	-0.0287 + 0.0153i	0 + 0.0325i	0.0287 + 0.0153i	0.0270 - 0.0181i	-0.0032 - 0.0324i
55	-0.0124 - 0.0301i	-0.0319 - 0.0063i	-0.0230 + 0.0230i	0.0063 + 0.0319i	0.0301 + 0.0124i	0.0270 - 0.0181i
56	0.0063 - 0.0319i	-0.0206 - 0.0251i	-0.033	-0.0206 + 0.0251i	0.0063 + 0.0319i	0.0287 + 0.0153i
57	1.4950 - 1.4950i	0.0000 - 2.1142i	-1.4950 - 1.4950i	-2.1142 - 0.0000i	-1.4950 + 1.4950i	-0.0000 + 2.1142i
58	0.0319 - 0.0063i	0.0206 - 0.0251i	0 - 0.0325i	-0.0206 - 0.0251i	-0.0319 - 0.0063i	-0.0287 + 0.0153i
59	0.0301 + 0.0124i	0.0319 - 0.0063i	0.0230 - 0.0230i	0.0063 - 0.0319i	-0.0124 - 0.0301i	-0.0270 - 0.0181i
60	0.0181 + 0.0270i	0.0287 + 0.0153i	0.033	0.0287 - 0.0153i	0.0181 - 0.0270i	0.0032 - 0.0324i
61	0.0000 - 2.0491i	-0.7842 - 1.8932i	-1.4490 - 1.4490i	-1.8932 - 0.7842i	-2.0491 - 0.0000i	-1.8932 + 0.7842i
62	-0.0181 + 0.0270i	-0.0094 + 0.0311i	0 + 0.0325i	0.0094 + 0.0311i	0.0181 + 0.0270i	0.0251 + 0.0206i
63	-0.0301 + 0.0124i	-0.0270 + 0.0181i	-0.0230 + 0.0230i	-0.0181 + 0.0270i	-0.0124 + 0.0301i	-0.0063 + 0.0319i
64	-0.0319 - 0.0063i	-0.0324 - 0.0032i	-0.033	-0.0324 + 0.0032i	-0.0319 + 0.0063i	-0.0311 + 0.0094i

Table 3 – The Look-up Table for Tracking (Continued)

Data #	Start at 13th Position	Start at 14th Position	Start at 15th Position	Start at 16th Position
1	-0.0230 - 0.0230i	-0.0230 - 0.0230i	-0.0230 - 0.0230i	-0.0230 - 0.0230i
2	0.0124 - 0.0301i	0.0153 - 0.0287i	0.0181 - 0.0270i	0.0206 - 0.0251i
3	0.033	0.0319 + 0.0063i	0.0301 + 0.0124i	0.0270 + 0.0181i
4	0.0124 + 0.0301i	0.0032 + 0.0324i	-0.0063 + 0.0319i	-0.0153 + 0.0287i
5	-1.4950 + 1.4950i	-1.9533 + 0.8091i	-2.1142 + 0.0000i	-1.9533 - 0.8091i
6	-0.0301 - 0.0124i	-0.0206 - 0.0251i	-0.0063 - 0.0319i	0.0094 - 0.0311i
7	0 - 0.0325i	0.0181 - 0.0270i	0.0301 - 0.0124i	0.0319 + 0.0063i
8	0.0301 - 0.0124i	0.0311 + 0.0094i	0.0181 + 0.0270i	-0.0032 + 0.0324i
9	1.4950 + 1.4950i	-0.0000 + 2.1142i	-1.4950 + 1.4950i	-2.1142 - 0.0000i
10	-0.0124 + 0.0301i	-0.0311 + 0.0094i	-0.0270 - 0.0181i	-0.0032 - 0.0324i
11	-0.033	-0.0181 - 0.0270i	0.0124 - 0.0301i	0.0319 - 0.0063i
12	-0.0124 - 0.0301i	0.0206 - 0.0251i	0.0319 + 0.0063i	0.0094 + 0.0311i
13	-1.4490 + 1.4490i	-1.8932 - 0.7842i	0.0000 - 2.0491i	1.8932 - 0.7842i
14	0.0301 + 0.0124i	-0.0032 + 0.0324i	-0.0319 + 0.0063i	-0.0153 - 0.0287i
15	0 + 0.0325i	-0.0319 + 0.0063i	-0.0124 - 0.0301i	0.0270 - 0.0181i
16	-0.0301 + 0.0124i	-0.0153 - 0.0287i	0.0270 - 0.0181i	0.0206 + 0.0251i
17	1.4490 + 1.4490i	-1.4490 + 1.4490i	-1.4490 - 1.4490i	1.4490 - 1.4490i
18	0.0124 - 0.0301i	0.0287 + 0.0153i	-0.0181 + 0.0270i	-0.0251 - 0.0206i
19	0.033	-0.0063 + 0.0319i	-0.0301 - 0.0124i	0.0181 - 0.0270i
20	0.0124 + 0.0301i	-0.0324 + 0.0032i	0.0063 - 0.0319i	0.0287 + 0.0153i
21	1.4490 - 1.4490i	0.7842 + 1.8932i	-2.0491 - 0.0000i	0.7842 - 1.8932i
22	-0.0301 - 0.0124i	0.0251 - 0.0206i	0.0063 + 0.0319i	-0.0311 - 0.0094i
23	0 - 0.0325i	0.0270 + 0.0181i	-0.0301 + 0.0124i	0.0063 - 0.0319i
24	0.0301 - 0.0124i	-0.0094 + 0.0311i	-0.0181 - 0.0270i	0.0324 + 0.0032i
25	-1.4490 - 1.4490i	2.0491 - 0.0000i	-1.4490 + 1.4490i	-0.0000 - 2.0491i
26	-0.0124 + 0.0301i	-0.0094 - 0.0311i	0.0270 + 0.0181i	-0.0324 + 0.0032i
27	-0.033	0.0270 - 0.0181i	-0.0124 + 0.0301i	-0.0063 - 0.0319i
28	-0.0124 - 0.0301i	0.0251 + 0.0206i	-0.0319 - 0.0063i	0.0311 - 0.0094i
29	0.0230 - 0.0230i	-0.0124 + 0.0301i	0.0000 - 0.0325i	0.0124 + 0.0301i
30	0.0301 + 0.0124i	-0.0324 - 0.0032i	0.0319 - 0.0063i	-0.0287 + 0.0153i
31	0 + 0.0325i	-0.0063 - 0.0319i	0.0124 + 0.0301i	-0.0181 - 0.0270i
32	-0.0301 + 0.0124i	0.0287 - 0.0153i	-0.0270 + 0.0181i	0.0251 - 0.0206i

Table 3 – The Look-up Table for Tracking (Continued)

Data #	Start at 13th Position	Start at 14th Position	Start at 15th Position	Start at 16th Position
33	-0.0230 - 0.0230i	0.0230 + 0.0230i	-0.0230 - 0.0230i	0.0230 + 0.0230i
34	0.0124 - 0.0301i	-0.0153 + 0.0287i	0.0181 - 0.0270i	-0.0206 + 0.0251i
35	0.033	-0.0319 - 0.0063i	0.0301 + 0.0124i	-0.0270 - 0.0181i
36	0.0124 + 0.0301i	-0.0032 - 0.0324i	-0.0063 + 0.0319i	0.0153 - 0.0287i
37	-0.0230 + 0.0230i	0.0301 - 0.0124i	-0.0325 - 0.0000i	0.0301 + 0.0124i
38	-0.0301 - 0.0124i	0.0206 + 0.0251i	-0.0063 - 0.0319i	-0.0094 + 0.0311i
39	0 - 0.0325i	-0.0181 + 0.0270i	0.0301 - 0.0124i	-0.0319 - 0.0063i
40	0.0301 - 0.0124i	-0.0311 - 0.0094i	0.0181 + 0.0270i	0.0032 - 0.0324i
41	-1.4490 - 1.4490i	0.0000 + 2.0491i	1.4490 - 1.4490i	-2.0491 + 0.0000i
42	-0.0124 + 0.0301i	0.0311 - 0.0094i	-0.0270 - 0.0181i	0.0032 + 0.0324i
43	-0.033	0.0181 + 0.0270i	0.0124 - 0.0301i	-0.0319 + 0.0063i
44	-0.0124 - 0.0301i	-0.0206 + 0.0251i	0.0319 + 0.0063i	-0.0094 - 0.0311i
45	1.4950 - 1.4950i	-1.9533 - 0.8091i	-0.0000 + 2.1142i	1.9533 - 0.8091i
46	0.0301 + 0.0124i	0.0032 - 0.0324i	-0.0319 + 0.0063i	0.0153 + 0.0287i
47	0 + 0.0325i	0.0319 - 0.0063i	-0.0124 - 0.0301i	-0.0270 + 0.0181i
48	-0.0301 + 0.0124i	0.0153 + 0.0287i	0.0270 - 0.0181i	-0.0206 - 0.0251i
49	1.4490 + 1.4490i	1.4490 - 1.4490i	-1.4490 - 1.4490i	-1.4490 + 1.4490i
50	0.0124 - 0.0301i	-0.0287 - 0.0153i	-0.0181 + 0.0270i	0.0251 + 0.0206i
51	0.033	0.0063 - 0.0319i	-0.0301 - 0.0124i	-0.0181 + 0.0270i
52	0.0124 + 0.0301i	0.0324 - 0.0032i	0.0063 - 0.0319i	-0.0287 - 0.0153i
53	-1.4950 + 1.4950i	0.8091 + 1.9533i	2.1142 + 0.0000i	0.8091 - 1.9533i
54	-0.0301 - 0.0124i	-0.0251 + 0.0206i	0.0063 + 0.0319i	0.0311 + 0.0094i
55	0 - 0.0325i	-0.0270 - 0.0181i	-0.0301 + 0.0124i	-0.0063 + 0.0319i
56	0.0301 - 0.0124i	0.0094 - 0.0311i	-0.0181 - 0.0270i	-0.0324 - 0.0032i
57	1.4950 + 1.4950i	2.1142 + 0.0000i	1.4950 - 1.4950i	0.0000 - 2.1142i
58	-0.0124 + 0.0301i	0.0094 + 0.0311i	0.0270 + 0.0181i	0.0324 - 0.0032i
59	-0.033	-0.0270 + 0.0181i	-0.0124 + 0.0301i	0.0063 + 0.0319i
60	-0.0124 - 0.0301i	-0.0251 - 0.0206i	-0.0319 - 0.0063i	-0.0311 + 0.0094i
61	-1.4490 + 1.4490i	-0.7842 + 1.8932i	-0.0000 + 2.0491i	0.7842 + 1.8932i
62	0.0301 + 0.0124i	0.0324 + 0.0032i	0.0319 - 0.0063i	0.0287 - 0.0153i
63	0 + 0.0325i	0.0063 + 0.0319i	0.0124 + 0.0301i	0.0181 + 0.0270i
64	-0.0301 + 0.0124i	-0.0287 + 0.0153i	-0.0270 + 0.0181i	-0.0251 + 0.0206i

Table 3 – The Look-up Table for Tracking (Continued)

5.2 Carrier Frequency Offset Estimation

As 802.11a standard describes that the "Short" symbols are for coarse estimation of the carrier frequency offset error and the "Long" symbols are for the fine estimation, this project approach also follows the same principle to research for an approach in estimating the carrier frequency offset.

As the previous description about carrier frequency offset, Equation **(6)** shows the effect of the frequency offset. Estimation of f_{off} in term of δk is by the mean of a special training sequence.

Assume L samples of a training sequence that contains 2 identical symbols starting with i. A correlation is formed as below.

$$Z_{\frac{L}{2}} = \sum_{i=0}^{\frac{L}{2}-1} s_{n,i} \cdot s^*_{n,i+\frac{L}{2}} \qquad \textbf{(15)}$$

Substituting Equation **(6)** and taking a similar correlation as above, the correlation at the receiver is

$$\begin{aligned}
\hat{Z}_{\frac{L}{2}} &= \sum_{i=0}^{\frac{L}{2}-1} \hat{s}_{n,i} \cdot \hat{s}^*_{n,i+\frac{L}{2}} \\
&= \sum_{i=0}^{\frac{L}{2}-1} (\gamma_i \cdot \tilde{r}_{n,i} + w_{n,i}) \cdot (\gamma^*_{i+\frac{L}{2}} \cdot \tilde{r}^*_{n,i+\frac{L}{2}} + w^*_{n,i+\frac{L}{2}}) \\
&= \sum_{i=0}^{\frac{L}{2}-1} [(\gamma_i \cdot \tilde{r}_{n,i} \cdot \gamma^*_{i+\frac{L}{2}} \cdot \tilde{r}^*_{n,i+\frac{L}{2}}) + (w_{n,i} \cdot \gamma^*_{i+\frac{L}{2}} \cdot \tilde{r}^*_{n,i+\frac{L}{2}}) + (\gamma_i \cdot \tilde{r}_{n,i} \cdot w^*_{n,i+\frac{L}{2}}) \\
&+ (w_{n,i} \cdot w^*_{n,i+\frac{L}{2}})]
\end{aligned} \qquad \textbf{(16)}$$

The expected value of the correlation at the receiver is

$$
\begin{aligned}
E\{\hat{Z}_{\frac{L}{2}}\} &= E\{\sum_{i=0}^{\frac{L}{2}-1}[(\gamma_i \cdot \tilde{r}_{n,i} \cdot \gamma^*_{i+\frac{L}{2}} \cdot \tilde{r}^*_{n,i+\frac{L}{2}}) + (w_{n,i} \cdot \gamma^*_{i+\frac{L}{2}} \cdot \tilde{r}^*_{n,i+\frac{L}{2}}) \\
&+ (\gamma_i \cdot \tilde{r}_{n,i} \cdot w^*_{n,i+\frac{L}{2}}) + (w_{n,i} \cdot w^*_{n,i+\frac{L}{2}})]\} \\
&= E\{\sum_{i=0}^{\frac{L}{2}-1}[(\gamma_i \cdot \tilde{r}_{n,i} \cdot \gamma^*_{i+\frac{L}{2}} \cdot \tilde{r}^*_{n,i+\frac{L}{2}})\} \\
&= E\{\sum_{i=0}^{\frac{L}{2}-1}(e^{j\frac{2\pi\delta k i}{N}} \cdot \tilde{r}_{n,i} \cdot e^{-j\frac{2\pi\delta k(i+\frac{L}{2})}{N}} \cdot \tilde{r}^*_{n,i+\frac{L}{2}})\} \\
&= e^{-j\frac{\pi\delta k L}{N}} \cdot E\{\sum_{i=0}^{\frac{L}{2}-1}(\tilde{r}_{n,i} \cdot \tilde{r}^*_{n,i+\frac{L}{2}})\} \\
&= e^{-j\frac{\pi\delta k L}{N}} \cdot \sum_{i=0}^{\frac{L}{2}-1}(s_{n,i} \cdot s^*_{n,i+\frac{L}{2}}) \\
&= e^{-j\frac{\pi\delta k L}{N}} \cdot Z_{\frac{L}{2}}
\end{aligned}
\tag{17}
$$

Taking the argument of $E\{\hat{Z}_{\frac{L}{2}}\}$, the carrier offset is obtained by

$$
\arg\{E[\hat{Z}_{\frac{L}{2}}]\} = -\frac{\pi \cdot \delta k \cdot L}{N} \tag{18}
$$

Finally, the carrier frequency offset is estimated by

$$
\hat{\delta k} = -\arg\{\hat{Z}_{\frac{L}{2}}\} \cdot \frac{N}{\pi \cdot L} \tag{19}
$$

where N equals the length of FFT, and L is the total length in time of the two identical symbols.

5.2.1 Coarse Estimation

As the property of the "Short" preamble, there are 10 repetitions of 16 samples per symbol. Therefore, the same correlation approach can be applied to the "Short" preamble between two adjacent symbols.

Let $\frac{L}{2} = 16$ be the sample length in time of a "Short" symbol. The receiver computes the correlation between two adjacent symbols according to

$$\hat{Z}_{Short} = \sum_{i=1}^{16} \hat{s}^*_{n,i} \cdot \hat{s}_{n,i+16} \tag{20}$$

By computing the argument of the correlations, the carrier frequency offset is estimated by

$$\hat{\delta k}_{2Short} = -\arg\{\hat{Z}_{Short}\} \cdot \frac{N}{\pi \cdot L} \tag{21}$$

where $N = 64$, and $L = 32$.

Since there are totally 10 symbols in the "Short" preamble, maximum 9 correlations can be taken from the preamble samples. Therefore, averaging 9 estimates gives a more precise carrier frequency offset estimate.

$$\hat{\delta k}_{10Short/9corr} = \frac{1}{9} \sum_{i=1}^{9} \hat{\delta k}_{2Short,i} \tag{22}$$

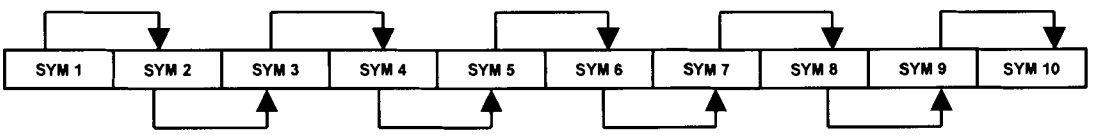

Figure 9 – 9 Correlations from 10 "Short" Symbols

Similarly, another approach is suggested by using two symbols with larger separations between them as the correlation arrangements as in Figure 10.

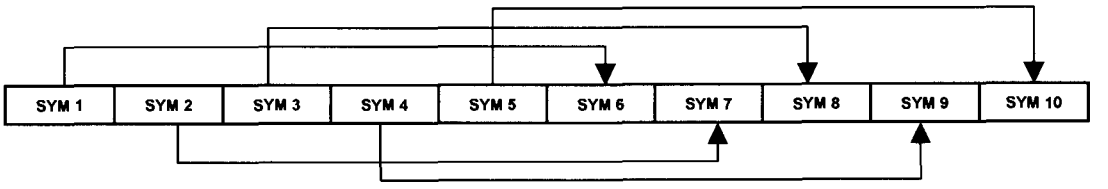

Figure 10 – 5 Correlations from 10 "Short" Symbols

The receiver computes the correlation between two adjacent symbols according to

$$\hat{Z}_{Short} = \sum_{i=1}^{16} \hat{s}^{*}_{n,i} \cdot \hat{s}_{n,i+16*5} \tag{23}$$

By averaging the 5 estimates from 5 correlations, the final estimate is given by

$$\hat{\delta k}_{10Short/5corr} = \frac{1}{5}\sum_{i=1}^{5} \hat{\delta k}_{2Short,i} \tag{24}$$

Since the "Short" preamble can also be interpreted as the structure similar to the "Long" symbols that consists of two 64-sample symbols plus a guard interval, the conventional correlation approach as Schmidl's method [9] is also examined as a reference for comparison.

The conventional method uses $\frac{L}{2} = 64$ be the sample length for the correlation.

The receiver computes the correlation between two adjacent symbols according to

$$\hat{Z}_{Short} = \sum_{i=1}^{64} \hat{s}^{*}_{n,i+32} \cdot \hat{s}_{n,i+32+64} \tag{25}$$

Compared to the conventional approach, the proposed algorithm in Figure 9 simplifies the number of data involved in correlations but increases the number of correlations; the proposed algorithm looks promising to improve the accuracy of estimation.

5.2.2 Fine Estimation

The plots in Figure 7 show the "Long" preamble contains only 2 symbols and each symbol has 64 samples. The carrier frequency offset can be estimated using the same approach above. Since there is a 32-sample guard interval, the total usable length of the "Long" symbols is 128 samples for 2 symbols.

The receiver computes the correlation between two "Long" symbols according to

$$\hat{Z}_{Long} = \sum_{i=1}^{64} \hat{s}^*_{n,i+32} \cdot \hat{s}_{n,i+32+64} \tag{26}$$

and estimates the carrier offset by

$$\delta\hat{k}_{2Long} = -\arg\{\hat{Z}_{Long}\} \cdot \frac{N}{\pi \cdot L} \tag{27}$$

where $N = 64$, and $L = 128$.

The coarse estimation uses the "Short" symbols to calculate the coarse carrier frequency offset value. Once a coarse estimate is obtained, the fine estimation fine-tunes the value to obtain a more precise estimate. The proposed approach to tackle the fine estimation uses the relationship below.

$$Estimation_{Fine} = Estimation_{Coarse} + Estimation_{Error} \tag{28}$$

The fine-tuning process means to estimate the error between the true value and the coarse estimated value of the carrier frequency offset. The suggested fine estimation approach applies the coarse estimate obtained from the "Short" symbols to partially get rid of the carrier frequency offset exits in the "Long" symbols. Since the carrier frequency offset is not completely removed, the correlation in Equation **(26)** is used to compute the remaining carrier frequency offset that is the estimation error in Equation **(28)**.

6. SIMULATION MODELS AND APPROACHES

6.1 Generation of OFDM Signal

6.1.1 "Short" Preamble and "Long" Preamble

The "Short" and "Long" preambles are created by taking the IFFT conversion with windowing of the "Short" sequence $\mathcal{S}$ and the "Long" sequence $\mathcal{L}$ as described in the paragraphs in section 4.1 and 4.2 respectively.

6.1.2 Signal and Data Fields

For simplicity reason, the "Signal" and "Data" fields are generated from a set of random data and periodically extended with the addition of the 16-sample guard intervals. The "Signal" field contains 80 OFDM signal samples, and each single "Data" field contains 80 OFDM signal samples.

6.2 Indoor Radio Channel Model [3]

In a mobile wireless system, Doppler shift and multipath fading are the major contributions cause the rapid fluctuation of the received signal amplitudes. Doppler shift is caused by the movement of the mobile terminal towards or away from the base terminal. In a multipath system, the received signals arrive from multiple paths with different phases, and the phases change rapidly when the mobile terminal is moving. The phase differences are caused by the different distances of travelling to the receiver through different arriving paths. The phase changes are commonly modelled as random variables with the Rayleigh distribution or Ricean distribution. The Rayleigh fading

model assumes that all signals suffer nearly the same attenuation in different arriving paths. The Ricean fading model considers a system has a strong Line of Sight (LOS) signal component.

In a wideband system, the transmitted signals are narrow pulses, and they arrive with different amplitudes and time delays. ISI happens if the multipath delay spread is comparable to or larger than the symbol duration. The amplitudes and time delays are random variables, and can be modelled as the delay power spectrum given by the impulse response

$$h(t) = \sum_{i=0}^{L} \alpha_i \delta(t - \tau_i) e^{j\varphi_i} \qquad \textbf{(29)}$$

where α_i is a Rayleigh distributed amplitude of the multipath with a mean local strength $E\{\alpha_i\} = 2\sigma_i^2$, τ_i is the delay time of the multipath arrival, φ_i is the phase of the multipath arrival, which is assumed to be uniformly distributed in $(0,2\pi)$.

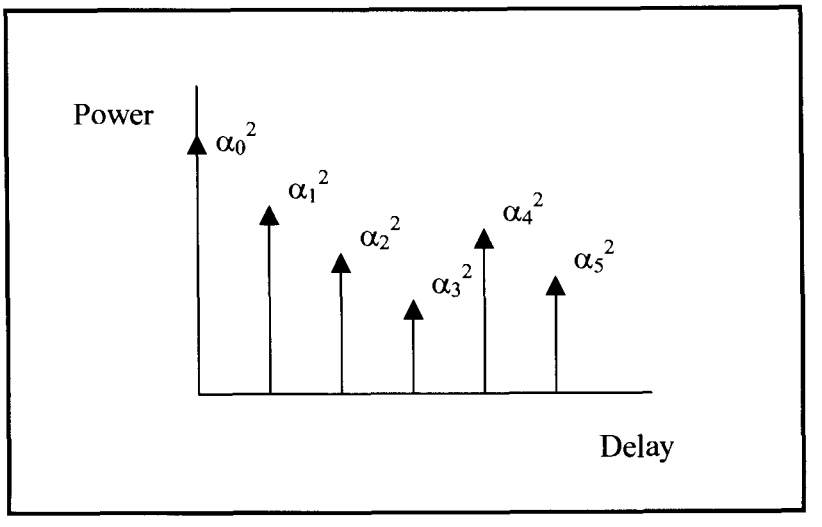

Figure 11 – Delay Power Spectrum

The general characterization of a multipath channel is described by the scattering function.

$$S(\tau;\lambda) = Q(\tau) \cdot D(\lambda) \qquad \textbf{(30)}$$

where $Q(\tau)$ is the delay power spectrum and $D(\lambda)$ is the Doppler Spectrum.

Joint Technical Committee (JTC) proposed wideband multipath channel models using the delay power spectrum models. The suggested models provide the relative time delays and the mean square values of the amplitudes for indoor commercial buildings, indoor office buildings, and indoor residential buildings. There are channel A, B, and C models associated with good, medium, and bad conditions respectively for each type of indoor environments.

	Channel A		**Channel B**		**Channel C**		
	Rel	**Avg**	**Rel**	**Avg**	**Rel**	**Avg**	**Doppler**
	Delay	**Power**	**Delay**	**Power**	**Delay**	**Power**	**Spectrum**
Tap	(nSec)	(dB)	(nSec)	(dB)	(nSec)	(dB)	D(l)
1	0	0	0	0	0	0	FLAT
2	100	-13.8	100	-6	100	-0.2	FLAT
3			200	-11.9	200	-5.4	FLAT
4			300	-17.9	400	-6.9	FLAT
5					500	-24.5	FLAT
6					600	-29.7	FLAT

Table 4 – JTC Multipath Indoor Residential Buildings Models

This project focuses on indoor residential applications; and therefore, the JTC wideband multipath channel B model in Table 4 for indoor residential buildings is applied in the simulations. Assuming that the Doppler Spectrum is flat and equals to 1, the JTC channel B model for indoor residential buildings is a 4 tapped delay lines model in Figure 12.

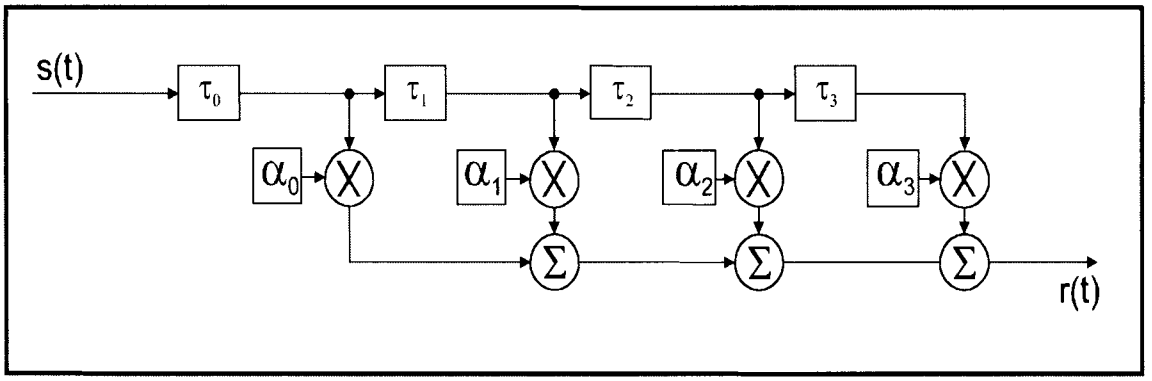

Figure 12 – Tapped Delay Lines Model

$$r(t) = \sum_{i=0}^{3} \alpha_i \cdot s(t-\tau_i) \cdot e^{j\varphi_i} = \alpha_0 \cdot s(t) + \sum_{i=1}^{3} \alpha_i \cdot s(t-\tau_i) \cdot e^{j\varphi_i} \qquad \textbf{(31)}$$

where $\alpha_0 \cdot s(t)$ represents the LOS components, $\sum_{i=1}^{3} \alpha_i \cdot s(t-\tau_i) \cdot e^{j\varphi_i}$ represents the NLOS (Near Line of Sight) components, $\alpha_i = \sqrt{Power_{avg,i}}$ is the amplitude of the $i-th$ arriving path, φ_i is the random phase, which is uniformly distributed in $(0,2\pi)$, of the $i-th$ arriving path.

6.3 AWGN Channel [11]

At the beginning of the simulation, energy per bit to the noise power density, Eb/No, is specified in dB to determine AWGN channel condition. Based on the Eb/No ratio, the signal power and noise power is determined by Equation **(32)** below.

$$\frac{C}{N} = \frac{E_b \cdot R}{N_o \cdot B} \tag{32}$$

where E_b is the energy per bit, R is the bit rate in bit/sec, N_o is the noise power density, is the modulation bandwidth in Hz. The modulation bandwidth equals to a half of the transmission bandwidth B_T.

$$B = \frac{B_T}{2} \tag{33}$$

Symbol rate, in symbol/sec, is defined as

$$D = \frac{R}{l} \tag{34}$$

where l is the number of bits per symbol.

Symbol time, in sec, of M-ary Phase Shift Keying equals

$$T = 1/D \tag{35}$$

Transmission bandwidth of MPSK equals to

$$B_T = 2 \cdot \frac{1}{T} \tag{36}$$

Therefore, the modulation bandwidth can be determined and equals to

$$B = D = \frac{R}{l} \tag{37}$$

The modulation bandwidth is used for calculating the signal to noise power ratio defined in Equation **(32)**.

Signal Power

$$C = E_b \cdot R = R \cdot \sum_{i=0}^{L-1} s_{n,i} \cdot s^*_{n,i} \tag{38}$$

where L is the length of the samples, $s_{n,i}$ is the signal level of the i-th sample of the OFDM symbol , and $s^*_{n,i}$ is its conjugate.

Noise Power

$$N = \frac{C \cdot B}{Eb/No \cdot R} = \frac{C \cdot D}{Eb/No \cdot R} \tag{39}$$

or if Eb/No is in dB,

$$N = \frac{C \cdot D}{R} \cdot 10^{-\frac{Eb/No}{10}} \tag{40}$$

Since the noise level is determined by taking the square root of the noise power, an attenuation factor G is defined here for calculating the noise levels of OFDM signal samples introduced by the AWGN channel using the relationship below.

$$G = \sqrt{N} \tag{41}$$

The simulation uses RANDN function to generate a set of Pseudo-random numbers for the additive AWGN noise. The Pseudo-random numbers are chosen from a normal distribution with zero mean, variance and standard deviation equals one. Multiply the attenuation factor with the Pseudo-random numbers generates the random noise data points. Finally, adding the random noise to the original sequence creates the noisy version of the OFDM sequence.

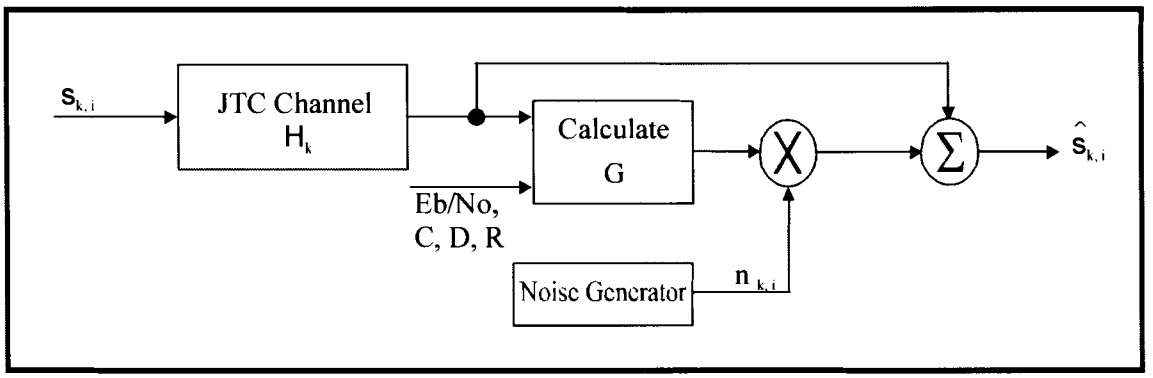

Figure 13 – AWGN Channel Model

7. SIMULATION AND RESULT

7.1 Time Offset Estimation

Figure 14 shows the simulation model to evaluate the performance of the proposed time/frame synchronization algorithm.

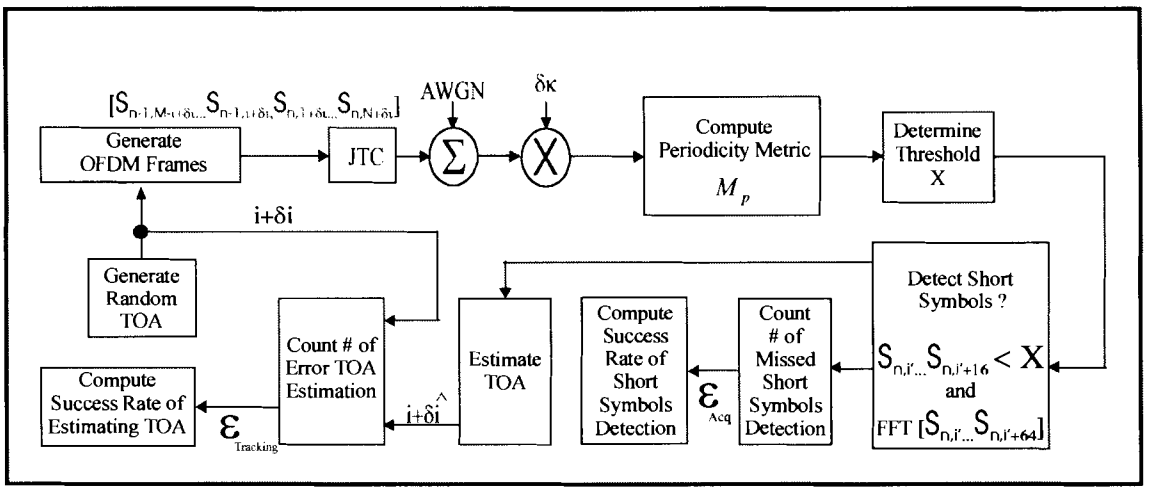

Figure 14 – Time Synchronization Simulation Model

The simulation generates a random number that is within 1 to 64 to determine the TOA of a current OFDM data frame starting with 10 "Short" symbols, and consists of 2 "Long" symbols, "Signal", and "Data" fields. Attaching a randomly generated "Data" symbol, as the data in a previous frame, to the current data frame according to the random TOA creates an OFDM data stream for simulations. The OFDM data stream goes through JTC channel with the addition of AWGN noise and carrier frequency offset δk. The receiver computes the periodicity metric and monitors the arrival of the "Short" symbols by a threshold detection.

After the receiver detects the presence of the "Short" symbols during acquisition, the simulations continue tracking the start position of the FFT window determined by the threshold detection. Tracking the start position of the FFT window is an important step to estimate the TOA and align the OFDM frame. Comparing the frequency domain data samples with the look-up table in the Table 3 using Minimum MSE by Equation **(14)** determines the start of the FFT window, and the TOA can be estimated accordingly.

The time offset estimation algorithm is evaluated with Monte Carlo approach with running 5000 times for each simulated conditions. The simulations study different threshold settings, including the levels at 1/3, 1/4, 1/5, 1/8 of the maximum range of the periodicity metric, in order to determine the best choice of the threshold at which the receiver can detect the periodic "Short" symbols most effectively during acquisition under different signal strengths and carrier frequency offsets. The simulations count for the number of times that the "Short" symbols detections are missed, and the success rates, in percentage, of the "Short" symbols detection during acquisition are presented after the simulations in order to determine the effectiveness of the detection under different threshold settings.

The simulations apply the best choice of the threshold, based on the simulations result during acquisition, and count for the number of times that the TOA estimations are incorrect under the influence of the carrier frequency offsets and different signal strengths. The mean and the standard deviation of the estimation errors of the TOA are computed. For evaluating the performance, the simulations present the success rate, in percentage, of estimating the actual TOA of the "Short" symbols; as well as, the mean and the standard deviation of the estimation errors.

7.1.1 Result

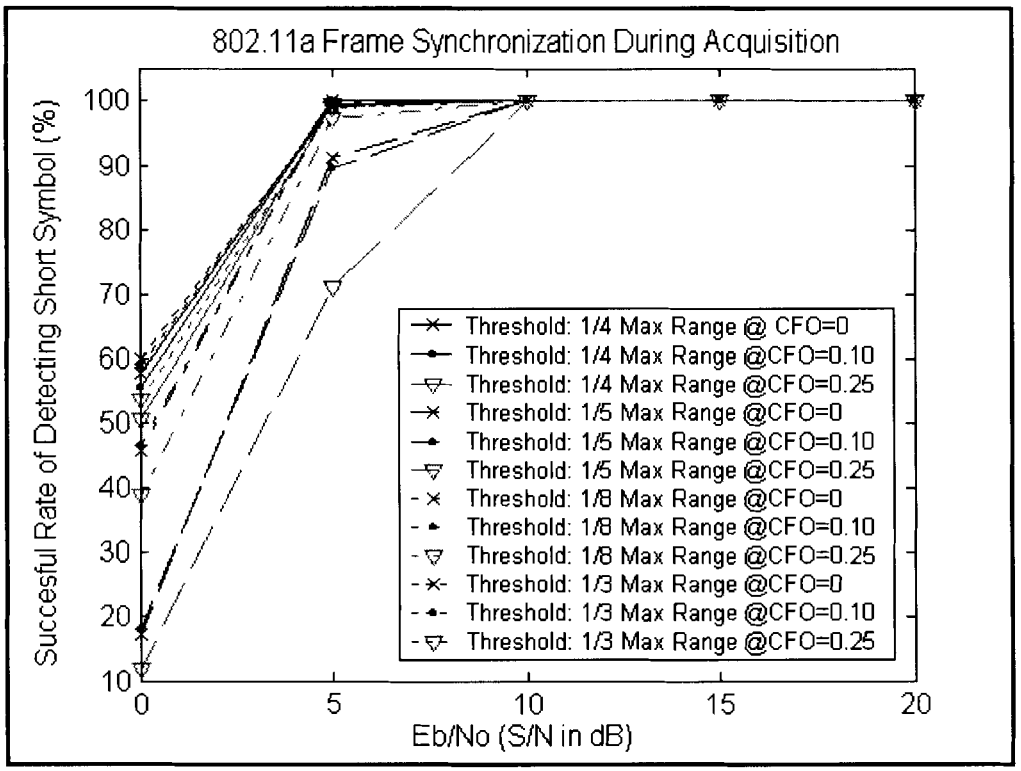

Figure 15 – "Short" Symbol Detection During Acquisition

Figure 15 shows the result that the algorithm can obtain the highest success rate at 0dB signal strength if the threshold is set to 1/3 of the maximum range of the periodicity metric. Under a poor signal strength condition, the success rate of detecting the "Short" symbols is higher when the threshold is set higher. However, the performance is getting poorer as the signal strength is getting stronger because of the wrong detection that caused by the threshold is set too high and hits the region contains uncorrelated signal. If the threshold is set to 1/4 of the maximum range of the periodicity metric, the results show that the algorithm can obtain a higher success rate when the signal strength is at or above 5dB. From the simulations, the results conclude that the optimum set point for the threshold is at the quarter point of the maximum range. Since the acquisition is the first

stage of the time/frame synchronization, the success of detecting the TOA and aligning the frame correctly depend on the highest success rate of detecting the arrival of the "Short" symbols. The following simulation results during tracking are based on setting the threshold to the quarter point of the maximum range of the periodicity metric.

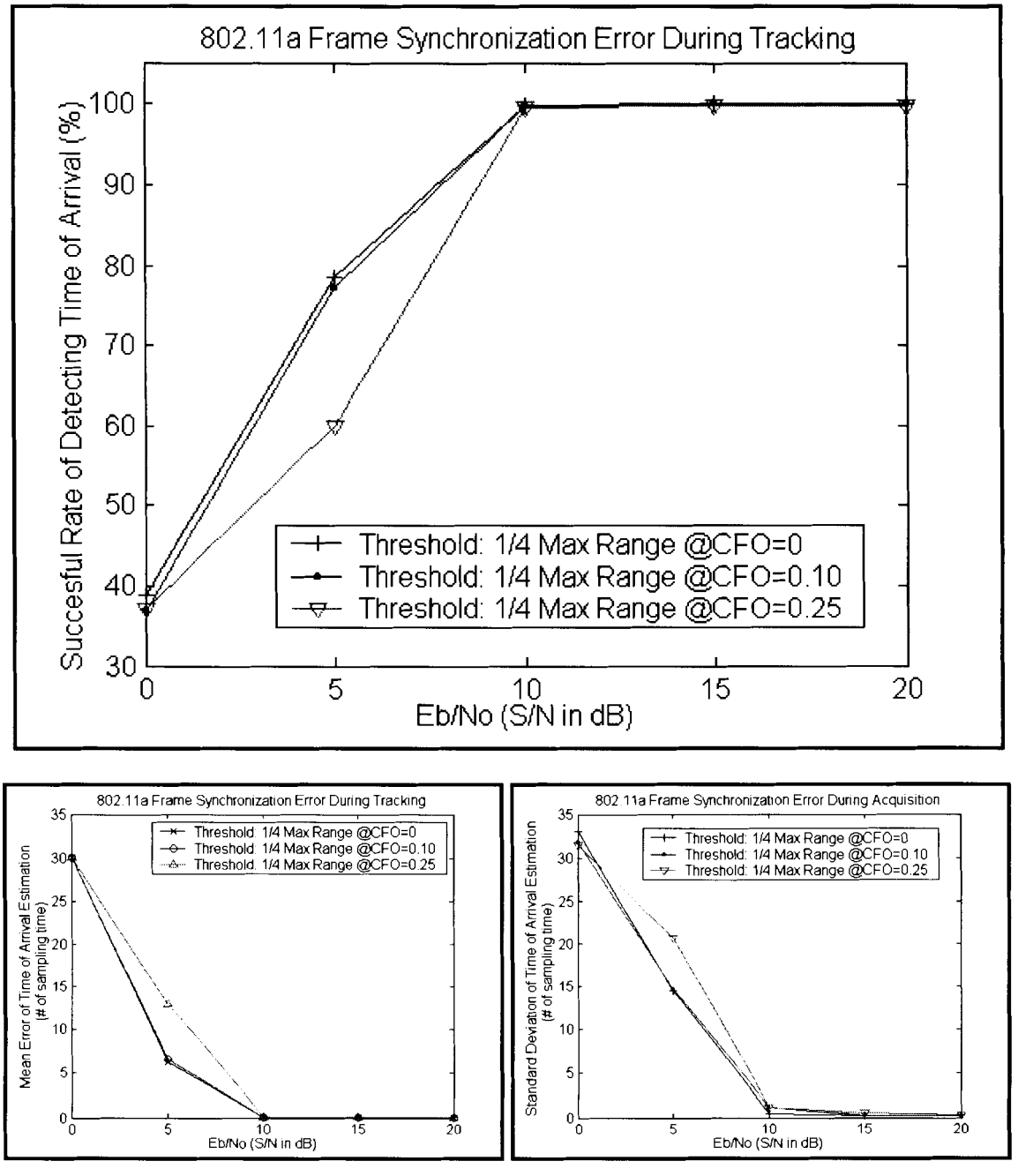

Figure 16 – Time of Arrival Estimation During Tracking

Figure 16 shows the results that the proposed algorithm for the time/frame synchronization works successfully. The estimation errors of the TOA reduce as the signal strength increases, and the algorithm performs effectively with the signal to noise ratio is greater than 10dB. Also, the influence of the carrier frequency offset causes a slightly degradation of the TOA estimate during the acquisition and tracking stages. At 20dB signal strength, the success rate of the TOA estimation is 99.94% with the carrier frequency offset equals to 0.25 of the frequency distance between subcarriers. The mean errors and the standard deviation errors of the TOA estimates show that the estimation is accurate with small spreads; in addition, the influence of the carrier frequency offset causes a slightly degradation of the mean errors and the standard deviation errors. At 20dB signal strength, the mean error is less than 0.01 of a sampling time, and the standard deviation error is less than 0.4 of a sampling time. The estimation errors are acceptable and may not cause a serious problem of detecting the OFDM frame data.

7.2 Carrier Frequency Offset Estimation

Figure 17 shows the Monte Carlo simulation approach on the proposed carrier frequency offset estimation algorithms.

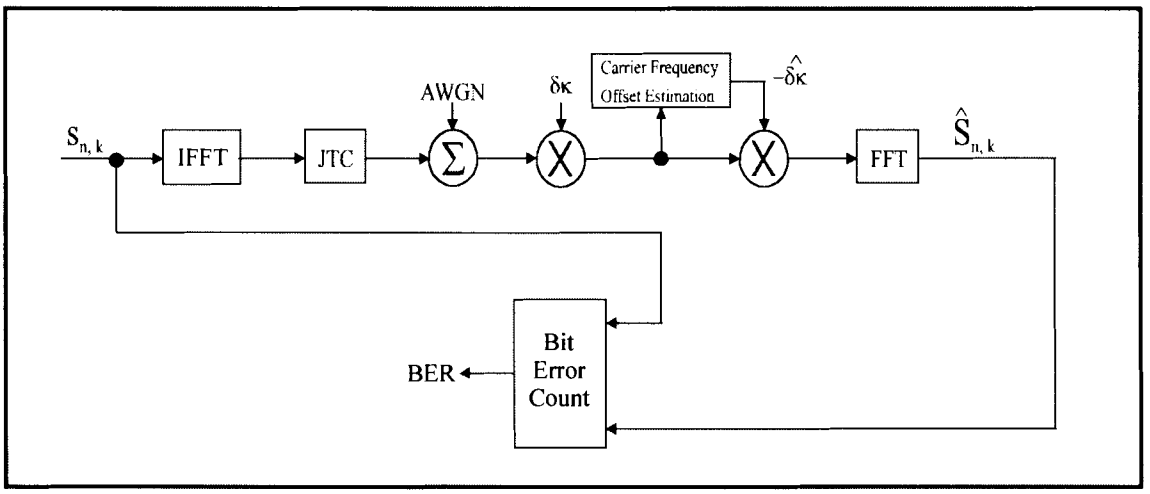

Figure 17 – CFO Simulation Model

Each simulation runs 2000 times for each simulated condition to obtain the mean estimates, the standard deviation of the estimates, the mean errors, the root mean square errors, the bit error rates (BER), and the frame error rates (FER) to evaluate the performance of different estimation methods. The simulations compare three methods for the coarse estimations and for the fine estimations of the carrier frequency offset.

The first method is the conventional method, which is named as "Method 1" in the simulation. This method coarsely computes the carrier frequency offset using two "Short" symbols with 64 samples for the correlation, and fine-tunes the estimates using both the coarse estimates and the correlation between two "Long" symbols of 64 samples each.

The second method is named as "Method 2" in the simulations, which coarsely computes the carrier frequency offset by averaging 9 correlations between two adjacent "Short" symbols. The fine estimation in "Method 2" applies the same method as in "Method 1", but uses a different method to obtain the coarse estimates.

The third method is named as "Method 3" in the simulations, which coarsely computes the carrier frequency offset by averaging 5 correlations between two "Short" symbols with 80 samples spaced between them. The fine estimation in "Method 3" also applies the same approach as in the other two methods.

The BER and FER analyses use a OFDM frame structure that consists of ten "Short" symbols, two "Long" symbols, one "Signal" symbol, and five "Data" symbols in addition of guard intervals. For the simplicity of the simulations, the data in "Signal" and "Data" fields are randomly generated in forms of QPSK without any coding scheme, and the OFDM data frame is assumed to be correctly synchronized in time and in frame. The main idea for the BER/FER simulations is to compare the number of error bits or frames when the "Signal" and "Data" fields in a data packet are compensated with carrier frequency offset estimates based on the three methods using both the "Short" and "Long" symbols. The simulations examine both a small quantity and a large quantity of carrier frequency offsets, and two sets of results are posted in Figure 18 and Figure 19.

7.2.1 Result

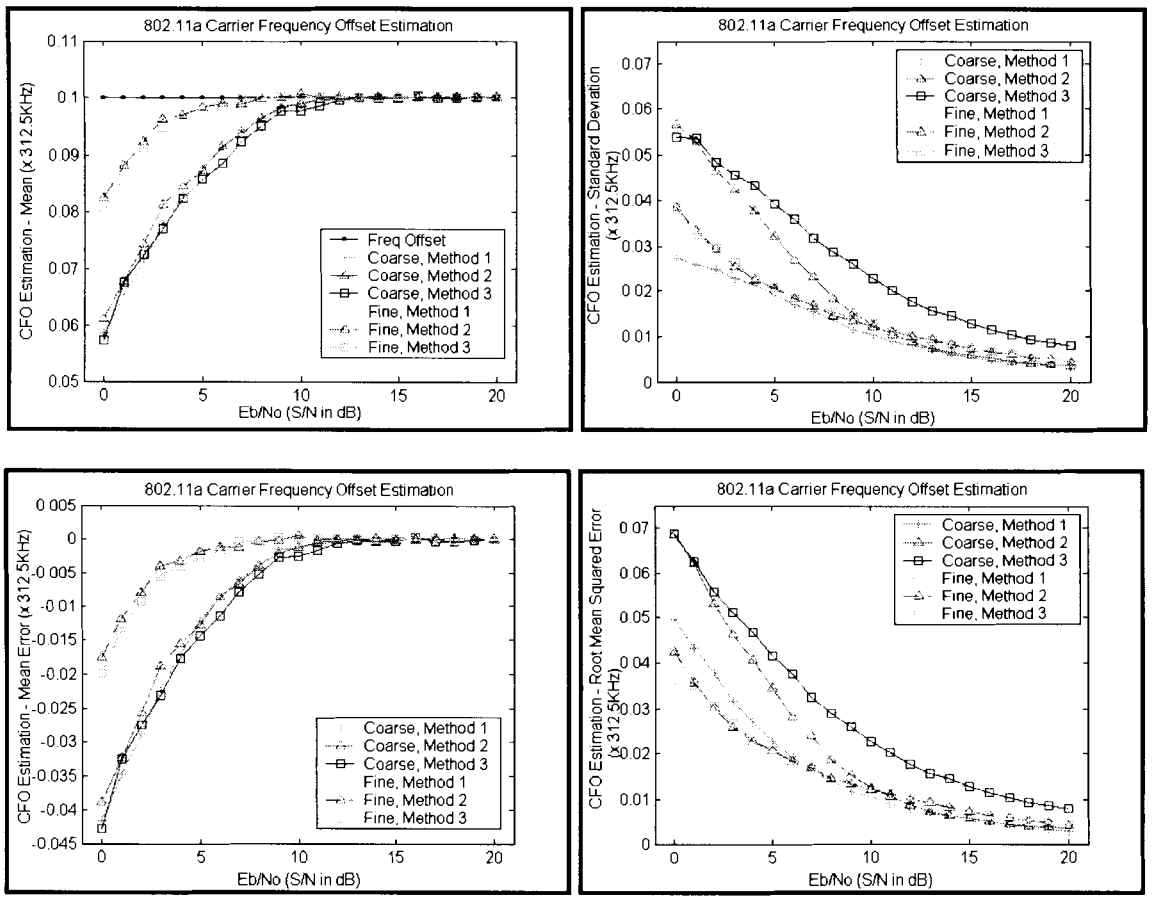

Figure 18 – Simulation CFO=0.1 x subcarrier frequency spacing

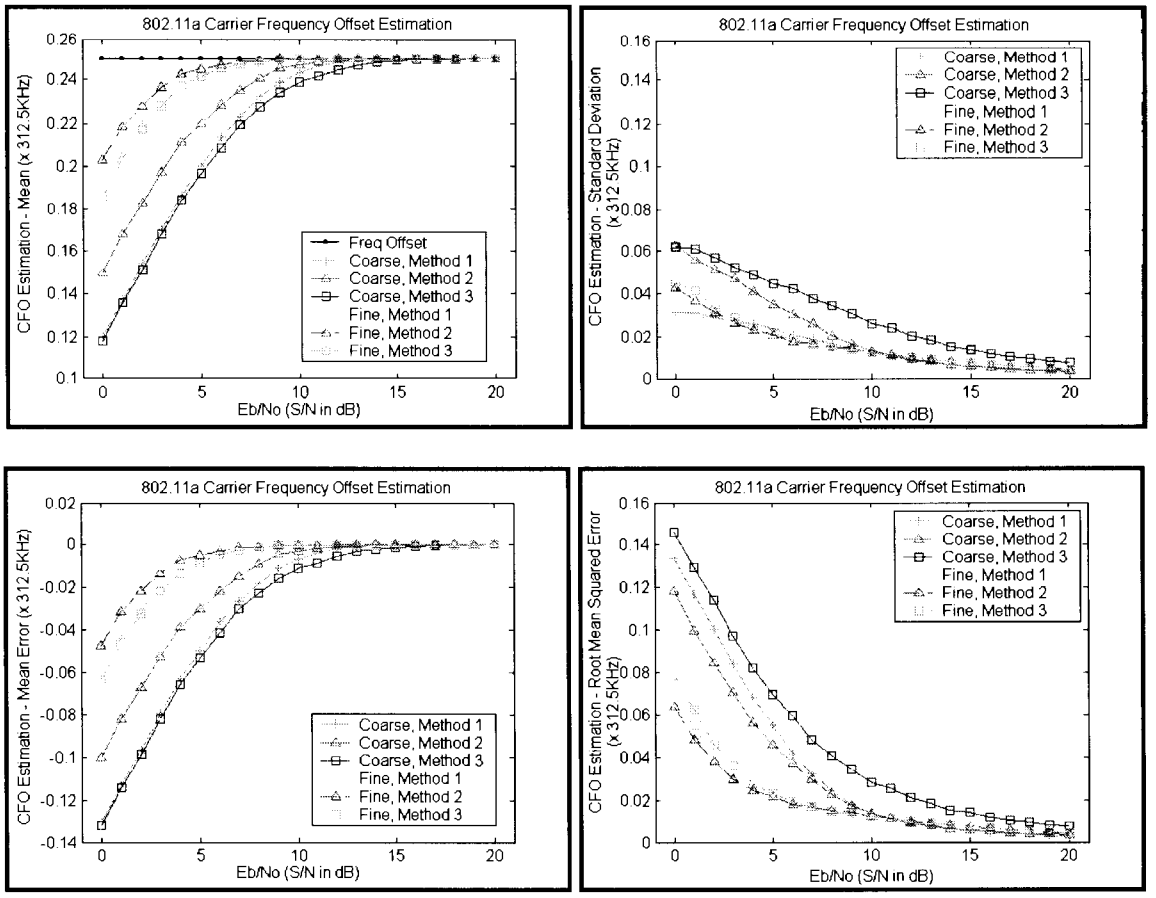

Figure 19 – Simulation CFO=0.25 x subcarrier frequency spacing

In Figure 18 and Figure 19, the results show that "Method 2", which coarsely computes the carrier frequency offset by averaging 9 correlations between two adjacent "Short" symbols, obtains the coarse estimates with the smallest mean errors compared to the other two methods. However, the spread of the coarse estimates in the "Method 2" increases compared to the "Method 1" if the signal to noise ratio drops below 10dB. The coarse estimates obtained from the "Method 1" has the smallest spread even through under a weak signal strength. The performances of the "Method 1" and the "Method 2" are compatible under the signal strength is greater than 10dB. The "Method 3" performs poorly compared to the other two methods.

The results also show that the proposed fine estimation approach improves the estimation of the carrier frequency offset, and the improvement has about 4 dB gain in signal to noise ratio compared to the coarse estimations of all the three methods. In addition, the "Method 2" obtains the fine estimates with the smallest mean errors compared to the other two methods. This observation indicates that the proposed fine estimation approach also depends on the coarse estimates.

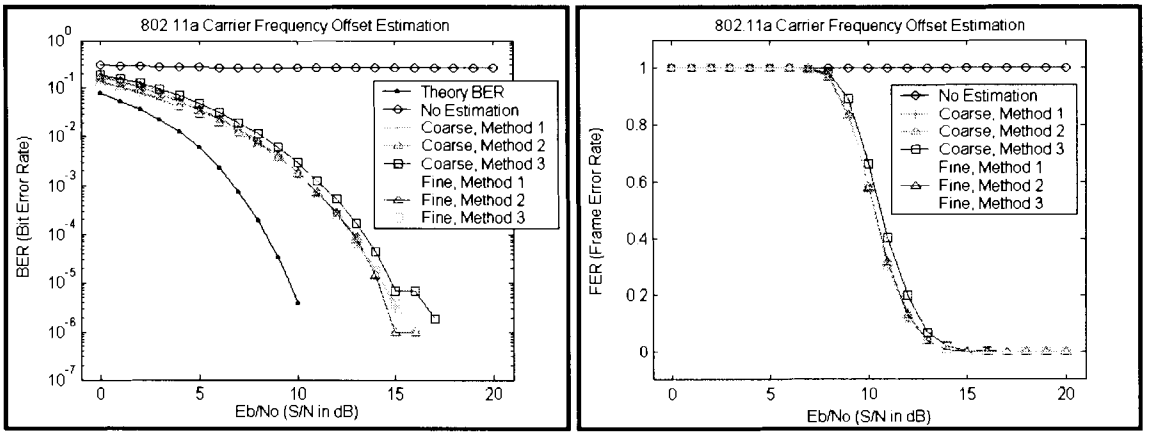

Figure 20 – BER / FER Simulations with CFO=0.1 x subcarrier frequency spacing

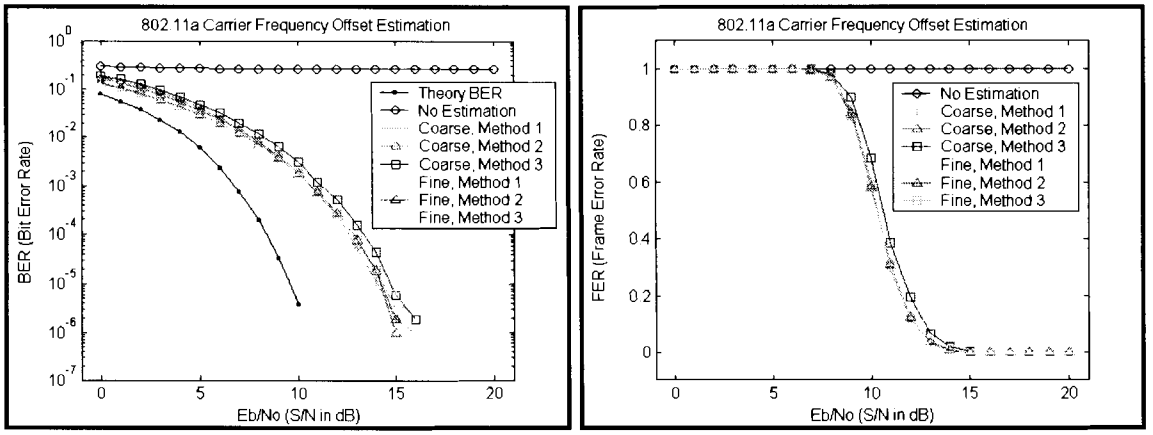

Figure 21 – BER / FER Simulations with CFO=0.25 x subcarrier frequency spacing

The results of measuring the BER and the FER in Figure 20 and Figure 21 shows that the performance of the "Method 2" is compatible with the conventional "Method 1" and is better than the "Method 3".

In conclusion, "Method 1" is the best choice, and the proposed "Method 2" can be an alternative method to obtain the coarse and the fine estimations of carrier frequency offset in 802.11a OFDM systems. The shorter length of corrections is the major advantage of the "Method 2".

8. CONCLUSION

The simulations in the project successfully show the effects of the carrier frequency offset on the time/frame synchronization and on the detection of the OFDM symbols in an 802.11a OFDM system under the AWGN and the JTC channels for an indoor residential environment. The simulations show the proposed algorithm for the time/frame synchronization performs well with high success rate of detecting the arrival of the "Short" symbols with acceptable errors in estimating the actual TOA.

The proposed coarse estimation algorithm as in the "Method 2", by averaging 9 correlations between two adjacent "Short" symbols, can be an alternative method for the carrier frequency offset estimations. The shorter length for correlations is the major advantage of the "Method 2", and the performance of the "Method 2" is compatible with the conventional "Method 1" after applying the proposed fine estimation algorithm. The fine estimation algorithm, which uses both the coarse frequency offset estimate and the correlation between two 64-sample "Long" symbols, improves the carrier frequency offset estimation significantly with less errors under a poor signal to noise ratio environment.

In an 802.11a system, the accuracy of the symbol timing and the correct alignment of the data frames are significant in reducing ISI and ICI. Therefore, the time/frame synchronization and the carrier frequency offset estimation work closely together in order to perform robustly in system synchronization.

Further research on synchronization suggested here is in the area of channel estimation using the "Long training sequence", which is mentioned in the 802.11a OFDM training structure. In addition, a study of the same synchronization algorithms under an outdoor wireless channel is also an interesting area.

REFERENCES

[1] R.W. Chang, "Synthesis of band-limited orthogonal signals for multi-channel data transmission", Bell Syst. Tech. J., vol. 45, pp. 1775-1796, Dec. 1966.

[2] IEEE LAN/MAN Standards Committee, "*IEEE Std 802.11a-1999*", IEEE, 1999.

[3] Kaveh Pahlavan, Prashant Krishnamurthy, "*Principles of Wireless Network*", Prentice Hall, 2002.

[4] Laszlo Hazy, Mohammed El-Tanany, "Synchronization of OFDM Systems Over Frequency Selective Fading Channels", *Proceedings of the IEEE Vehicular Technology Conference*, VTC97, Phoenix, Arizona, May 4-7, 1997

[5] Paul H. Moose, "A Technique for Orthogonal Frequency Division Multiplexing Frequency Offset Correction", *IEEE Transactions on Communications*, Vol. 42, No. 10, pp2908-2914, Oct. 1994

[6] Ashish Pandharipande, "Principles of OFDM", *IEEE Potentials, pp16-19,* April/May 2002

[7] Jan-Jaap van de Beek, "ML Estimation of Time and Frequency Offset in OFDM Systems", IEEE *Transactions on Signal Processing*, Vol. 45, No. 7, pp1800-1805, July 1997

[8] T. Kim, N. Cho, J. Cho, K. Bang, K.Kim, H. Park and D. Hong, "A Fast Burst Synchronization for OFDM Based Wireless Asynchronous Transfer Mode Systems", *IEEE Globecom,* Rio de Janeiro, Brazil, Dec. 5-9, 1999, pp543-548

[9] Timothy M. Schmidl and Donald C. Cox, "Robust Frequency and Timing Synchronization for OFDM", *IEEE Transactions on Communication*, Vol. 45, No. 12, pp1613-1621, Dec. 1997

[10] Andreas F. Molisch et. al., "*Wideband Wireless Digital Communications*", Prentice Hall, 2001

[11] Leon W. Couch II, "Digital and Analog Communication Systems", 3rd Edition, MacMillan, 1989

[12] M. Speth, F. Classen, and H. Meyr, "Frame Synchronization of OFDM Systems in Frequency Selective Fading Channels", *Proceedings of the IEEE Vehicular Technology Conference*, VTC97, Phoenix, Arizona, May 4-7, 1997, pp. 1807–1811.